THE ASTROPHYSICAL JOURNAL, 492:495–510, 1998 January 10
© 1998. The American Astronomical Society. All rights reserved. Printed in U.S.A.

A *COBE* MODEL OF THE GALACTIC BAR AND DISK

H. T. FREUDENREICH[1]

Received 1997 May 20; accepted 1997 August 21

ABSTRACT

A model of the bar and old stellar disk of the Galaxy has been derived from the survey of the Diffuse Infrared Background Experiment (DIRBE) of the *Cosmic Background Explorer* at wavelengths of 1.25, 2.2, 3.5, and 4.9 μm. It agrees very well with the data, except in directions in which the near-infrared optical depth is high. Among the conclusions drawn from the model is that the Sun is located approximately 16.5 pc above the midpoint of the Galactic plane. The disk has an outer edge 4 kpc from the Sun and is warped like the H I layer. It has a central hole roughly the diameter of the inner edge of the 3 kpc molecular cloud ring, and within that hole lies a bright, strong, "early-type" bar, tilted approximately 14° from the Sun–Galactic center line. The model has 47 free parameters. The model is discussed in detail, and contour plots and images of the residuals are presented.

Subject headings: diffuse radiation — galaxies: photometry — Galaxy: fundamental parameters — Galaxy: structure — infrared: galaxies

1. INTRODUCTION

Only in recent years has it become accepted that our Galaxy is barred. For decades, the prevailing assumption had been that the central concentration of stars, hidden by intervening dust, could be described by a spheroid in which the density of stars fell as a power of the distance from the center. So much was suggested by the distribution of globular clusters in the Galaxy and by the structure of elliptical galaxies and the apparent shape of the central bulges of many spiral galaxies viewed edge-on. What little observational evidence there was, obtained by counting stars in low-extinction windows toward the inner Galaxy, did not disprove this notion. Some examples of spheroidal bulge models may be found in de Vaucouleurs & Pence (1978), Bahcall & Soneira (1980), Kent (1992), and Zhao (1996).

Meanwhile, radio astronomy had been accumulating evidence that the inner part of the Galaxy is less neatly arranged. The radial velocities of gas in the inner few kiloparsecs was found to be inconsistent with travel in circular orbits. In some directions, the velocity is so great that the gas was proposed to lie in an "expanding 3 kpc arm" (Oort, Kerr, & Westerhout 1958) between us and the center; in general, its motion seemed predominantly outward, as if the gas were being driven by titanic explosions near the Galactic center (Burbridge & Hoyle 1963), but this notion lost favor as the improbably vast energy and driven mass required of such explosions came to be better understood (Sanders & Prendergast 1974).

An alternative explanation is that the gas is moving in noncircular orbits because the potential in which it lies is asymmetric, perhaps because of a bar, as de Vaucouleurs (1964) suggested. Others came to a similar conclusion, among them Liszt & Burton (1980) and Gerhard & Vietri (1986). Binney et al. (1991) took this analysis further. From the kinematics of H I, CO, and CS, they deduced the presence of a bar whose near end lay in the first Galactic quadrant, tilted $16° \pm 2°$ from the line joining the Sun and the Galactic center.

By this time, information from stars in the central part of the Galaxy had begun to arrive, mostly from observations in the mid- and near-infrared. Harmon & Gilmore (1986) constructed a picture of the shape of the stellar bulge by selecting Mira variables, whose period is a function of luminosity, from the *IRAS* point source catalog on the basis of color. They found the bulge to be flattened in Z, and, though they did not remark on it, the outer contours of their Figure 3*a* show the bulge to be broader at positive longitudes. Nakada et al. (1992), Whitelock & Catchpole (1992), and Weinberg (1992) also found this effect in the distribution of *IRAS* Mira variables and noted that it was consistent with the appearance of a bar with its near end in the first quadrant. More evidence came through the near-infrared. Matsumoto et al. (1982) had mapped the surface brightness of the bulge at 2.4 μm; the pattern of the longitudinal asymmetry of this map was read by Blitz & Spergel (1991) as the clear signature of a bar.

The Diffuse Infrared Background Experiment (DIRBE) of the *Cosmic Background Explorer* (*COBE*) mapped the entire sky in 10 wavelength bands, including four in the near-infrared (Boggess et al. 1990). Weiland et al. (1994) corrected the DIRBE 2.2 μm map for extinction and subtracted an extrapolated projection of the Galactic disk, leaving behind a boxy, very barlike object that seems to loom forward into the first quadrant. Dwek et al. (1995) applied a variety of bar and spheroid models to this same data and concluded that the bulge is definitely a bar, with a tilt angle of $20° \pm 10°$.

Gravitational microlensing has recently been proposed as a means of studying the inner Galaxy. Results from the OGLE project regarding the bar are still preliminary (Paczyński et al. 1994), but the stellar database assembled for the project has allowed Stanek et al. (1997) to discover a bar tilted 20°–30°.

Freudenreich (1996; hereafter Paper I), presented a model of the Galactic disk derived from the DIRBE observations at 1.25, 2.2, 3.5, and 4.9 μm, where the surface brightness is dominated by red giants. The DIRBE photometric bands approximate the standard J, K, L, and M bands. (Here the "D" subscript used to denote DIRBE in Paper I will be omitted.) The model presumed that mature stars and the diffuse component of the interstellar dust each form a homogeneous, possibly warped, disk; if the structure of the Galaxy appears different in different near-infrared bands, it is due solely to wavelength-dependent extinction and emis-

[1] Hughes STX, Code 685.9, NASA/Goddard Space Flight Center, Greenbelt, MD 20771; freudenreich@gsfc.nasa.gov.

sion by dust. The model fitted the data very well, except in the directions of nearby molecular clouds, for which a smooth dust model cannot account, and toward the inner 3–4 kpc of the Galaxy, which had been intentionally masked out to avoid the bulge. In this paper, I have used the same data but expanded the model to include the bulge and the inner part of the disk. The "young disk" (the "thin disk" in Paper I), the ragged collection of molecular clouds, young stars, and associated dust concentrated at the Galactic plane, makes penetration of the inner part of the Galaxy difficult, but in the near-infrared the extinction is low enough that, with the proper techniques, we can discern structure to within roughly 0.5 kpc of the center.

Subsequent sections discuss the data reduction and optimization scheme, the model itself, how well it fits the data, its residuals, and what it tells us about the Galaxy. There are frequent references to Paper I, in particular for a more detailed explanation of the data reduction and a review of the model parameters pertaining to the disk, but all the information needed to understand the model is included here. Comparison to others' work is made in the course of discussing the parameters of the model.

2. PROCEDURE

2.1. *Data Preparation*

The analysis was performed on cylindrical equal-area projections of the DIRBE full-sky surface brightness maps, each map consisting of 391,612 pixels. The zodiacal light was modeled and removed, and point sources (nearby stars and a few supergiants) were filtered out. (See Paper I for a more detailed explanation.) At low latitudes, $b < 20°$, unresolved sources dominate the DIRBE surface brightness, but, at higher latitudes, the contribution of point sources cannot be neglected. To account for the deleted point sources, the simplifying assumption was made that all stars within a "deletion distance" D_v of the Sun were filtered out, which in effect places us at the center of a star-free bubble. There are three deletion distances: one each for the J and K bands and one for both the L and M bands. The M band does not have its own deletion distance because it is seriously contaminated at high Galactic latitudes by zodiacal light or by artifacts of its removal.

Maps of the near-infrared colors were then used to identify and mask anomalously red areas of the sky, most of which are strongly associated with molecular clouds. The mask derived from the $K-L$ color has been retained from Paper I, without, of course, the rectangle covering the Galactic bulge. In the inner Galaxy, this mask covers everything within approximately 3° of the Galactic equator. A second mask, chosen on the basis of $J-K$ color, has been added for use with the J-band map only (see Fig. 1; from this point on, the term "primary mask" refers to both of these masks used in conjunction). The Magellanic Clouds and the heart of the Barnard 78 cloud complex ($l \approx 1°$, $b \approx 4°$) were excluded by rectangular masks.

Shrinking the masked area would certainly introduce more contamination by young-disk features, which the robust fitting procedure might or might not be able to accommodate, yet there are reasons to consider doing so. One is that we could approach the Galactic center more closely. Another is that the mask is an implicit parameter of the fit, and by using more than one we can gauge our sensitivity to it. As further justification, we may note that a line of sight at low latitude toward the inner Galaxy can accumulate a great deal of reddening solely from diffuse dust, for which the model is intended to account in an averaged way. Therefore I created a "minimal" mask. For $|l| > 60°$ or $|b| > 8°$, it is identical to the primary mask for all four bands, but interior to this only the Barnard 78 clouds and a narrow strip ($-1.°1 < b < 0.°9$) along the Galaxy's brightness crest, which has been eroded by point-source removal, are excluded.

As a further precaution against zodiacal light residue, a zone of low ecliptic latitude β was also rejected, regardless of mask, in the disk region. For J, K, and L, $|\beta| > 15°$; for M, $|\beta| > 20°$.

2.2. *The Optimization*

The maps were divided into bulge and disk regions. The bulge region is defined as $|b| < 12°$, $|l| < 20°$; the disk region is everywhere else. The model was optimized separately for multiple samples of pixels taken from the DIRBE maps. A sample of pixels was chosen, the fit made, its figures of merit and parameter values recorded, a new sample chosen, a new starting point in parameter space chosen at random, and the process repeated. The disk region was represented by 660 pixels, only 60 taken from $|b| > 20°$, where a line of sight spans a smaller portion of the Galactic plane. The bulge region was represented by 170 pixels, out of the possible 6795 which remain after the primary mask has been applied. The pixels comprising each sample were selected quasi-randomly, to ensure uniform spatial coverage without imposing the artificial regularity of a grid. In the disk region, the density of selected pixels was low enough that each sample was virtually unique, but in the bulge region some pixels were selected more than once, and some (5%) never. The results presented are the averages over fits to 60 samples, but, because of overlap between samples in the bulge region, this is no better than having only 37 independent samples of the same size. The number of pixels in the bulge region limits how well the mean of any given parameter can be determined.

In fitting the model, the figure of merit was calculated separately for each band in each of the two regions, then weighted means were taken to form a disk figure of merit and a bar figure of merit. In the disk region, M is the least trustworthy band because of residual zodiacal light, and K and L are the most trustworthy. I assigned bands J through M the relative weights 1.0, 2.0, 2.0, and 0.1, respectively. In the bulge region, zodiacal light residue is negligible and extinction makes J the least useful band. There I assigned the relative weights 0.1, 2.0, 3.0, and 3.0, respectively. Changing the relative weights in either region had little effect on the final result, as long as most of the weight was not given to either J in the bulge region or M in the disk region. The figures of merit for the disk and bar were then averaged to arrive at a single figure. The relative weights of the disk and the bulge proved unimportant. Few of the parameters significantly affected the quality of fit in both regions.

In Paper I, the figure of merit was not the χ^2 but a statistically robust quantity, $\psi \equiv \langle \mathrm{DATA}_j - \mathrm{MODEL}_j/\sigma_j \rangle$, where j denotes pixel number and the angle brackets denote a bisquare-weighted average over pixels. Unlike χ^2, ψ can accommodate small-scale irregularities in Galactic structure, such as the deep patchy extinction associated with molecular clouds, that remain even after applying the exclu-

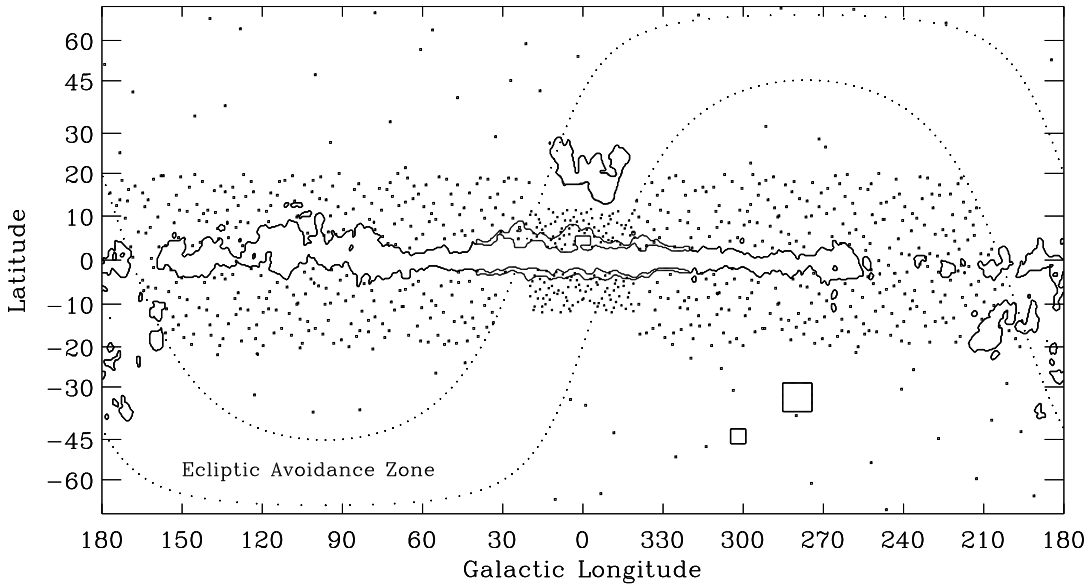

FIG. 1.—One sample of pixels selected for fitting the model. The area within the inner contours is rejected for being anomalously red. The area within the outer contours is rejected from only the J band. The dotted curves are at $\beta = \pm 15°$, within which zodiacal light residue may be significant.

sion mask and defy any smooth model. Another advantage of a robust figure of merit is that, by giving less weight to a lesser component, it aids in cleanly dividing the Galaxy into components: bar plus disk plus whatever appears in the final residuals. Estimates of the measurement errors σ_j were obtained from the scatter about polynomial fits to the local surface brightness (see Paper I). Although ψ has the basic characteristics desired of the figure of merit, it makes no quantitative statement about the validity of the model in any case, and it has been replaced by a measure that is simpler and at least makes more intuitive sense, the mean absolute fractional deviation (MAD), obtained by substituting DATA_j for σ_j in the equation above.

The optimization algorithm was based on the simulated annealing method (Press et al. 1992, p. 445). It never failed to converge.

3. THE MODEL

My intention was to build a simple model. I still consider the model simple, overly simple in some respects, but, grudgingly, parameter by parameter, it grew to a minimum of 47 free parameters. Seven pertain to the data reduction, 11 to the dust layer, 15 to the disk, 12 (to 14) to the bar, and two to the location of the Sun. A few of the symbols representing the parameters have been changed since Paper I in the interest of clarity, as their number has multiplied; these changes are noted in the text. The parameters are explained in the subsections that follow and are labeled later on when their values are tabulated.

Modeling was done in Galactocentric cylindrical coordinates (R, θ, Z), with the Sun at (R_0, 180°, Z_0), and θ measured counterclockwise, looking down from positive Z. The parameter Z_0 is free.

The model consists of an exponential stellar disk, a bar, and an exponential disk of diffuse dust. A thick disk is not included. As noted in Paper I, a thick disk is superfluous to reproducing the observed surface brightness. If one exists, it is too faint for the DIRBE to discern. After some experimentation with a halo model, a halo was rejected for the same reason.

The intensity at frequency ν in the direction (l, b) is obtained by integrating the volume emissivity ρ along the line of sight s,

$$I_\nu(l, b) = \delta_\nu + \int_{(l,b)} ds(\rho_\nu^{\mathrm{disk}} + \rho_\nu^{\mathrm{dust}} + \rho_\nu^{\mathrm{bar}}) e^{-\tau_\nu(s)} . \quad (1)$$

The additive offset δ_ν absorbs the extragalactic background and possibly zodiacal light and filtering artifacts. The extinction term $\exp[-\tau_\nu(s)]$ is calculated from the dust model.

3.1. *The Model of the Stellar Disk*

The modeled disk is exponential in R, outer truncated in R, inner truncated in R, sech^2 in Z, and warped. The model does not force the truncations and warping but allows them to occur if the data so dictate.

For $R \leq R_w$, another free parameter, the modeled disk is flat. For $R > R_w$, it is allowed to bend upward on one side and downward on the other, with a straight line of nodes at azimuth θ_w. Letting $u \equiv R - R_w$, the mean elevation from the flat reference plane established by the inner Galaxy is

$$\bar{Z}(R, \theta) = (c_1 u + c_2 u^2 + c_3 u^3) \sin(\theta - \theta_w) . \quad (2)$$

In Paper I, giving the disk a hole in its center, as in a Freeman type II galaxy (Freeman 1970), produced more plausible residuals than leaving it purely exponential. Holes have been found in the disks of other barred spirals (Ohta, Hamabe, & Wakamatsu 1990), though not all (Baggett, Baggett, & Anderson 1996), and this is a natural outcome in N-body simulations, in which a bar forms from an instability in the disk (Hohl 1971; Schwartz 1984; Noguchi 1996, and references therein). Therefore the modeled disk is permitted a central hole. Since the inner part of the disk cannot be expected to be axisymmetric in the presence of a strong bar, the hole is permitted an eccentricity. The hole is implemented through the function

$$H(R, \theta) = 1 - e^{-(R_H/O_R)^{O_N}} , \quad (3)$$

where O_N is real and $R_H^2 = X'^2 + (\varepsilon Y')^2$ is calculated in the bar frame, in which X' is defined by the bar's major axis.

The axis ratio of the hole is ε. This H was the best of three three-parameter functions tried and arose naturally from the best of several two-parameter functions, $H = 1 - \exp[-(R_H/O_H)^2]$. The function suggested by Freeman (1970), $H = \exp(R_{\min}^3/R^3)$ was not among the better two-parameter functions, being too steep. The less successful three-parameter functions were of logistic and algebraic forms.

The full expression for the volume emissivity of the disk in each of the four bands is

$$\rho_v^{\rm disk} = \rho_v^{\rm disk}(0) H e^{-R/h_r} \operatorname{sech}^2\left(\frac{Z-\bar{Z}}{h_z}\right), \tag{4}$$

where

$$h_r = \begin{cases} \text{a free parameter}, & R < R_{\max}; \\ 0.5 \text{ kpc}, & R > R_{\max}. \end{cases} \tag{5}$$

The truncation radius $R_{\max}$ and the central emissivity (in the absence of a hole) $\rho_v^{\rm disk}(0)$ are also free parameters. [The symbol "$\rho(0)$" replaces the "k" used in Paper I.]

The scale length h_r and scale height h_z are constant. This assumption may not be strictly valid in the outer Galaxy, where dark matter comes to dominate the mass. In particular, h_z may grow with R, as does the scale height of the H I layer (Burton 1976). I attempted to allow for this effect by including two additional parameters, a rate of change of h_z with R and a radius beyond which the change occurs. This proved fruitless. Whether the scale height was a function of R or of R^2, the additional freedom did not lead to a significant change in the figure of merit of the fit. It did allow the truncation radius $R_{\max}$ to be moved outward a kiloparsec or two but did not provide justification for the move or for itself and so was dropped.

3.2. *The Model of the Dust Layer*

The model of the dust layer is used to calculate extinction and emission by dust and possibly some of the light scattered by dust. The dust layer has the same form as the stellar disk, though with its own scale height (h_z^d), scale length (h_r^d), and hole parameters (O_R^d and O_N^d). The eccentricity of the dust layer's hole is forced to that of the disk. The dust layer is given a warp with the same line of nodes but an amplitude, $\bar{Z}^d = x^d \bar{Z}$, that differs by a scale factor x^d. This was done because Freudenreich et al. (1994) noted that, in surface brightness maps, the dust layer as observed in the far-infrared appears to be warped through a greater amplitude than the stellar disk and because the mean distances of the disk stars and the dust that is important to the model (foreground dust) may not be the same. Two changes have been made since Paper I. The radial dependence of the dust density, in the absence of a central hole, has been changed from 0.5 sech (R/h_r^d) to exp (R/h_r^d) to be consistent with the form of the stellar disk; in addition, because of the greater sensitivity to extinction now that more of the inner Galaxy is included, the extinction law of Rieke & Lebofsky (1985) has been replaced by a power law in wavelength, $A_\lambda = A_J(\lambda/1.25)^{-\alpha}$, where A_J and α are free.

It is likely that the scale height of the dust layer, like that of the H I layer, grows outside the solar circle, but the optical depth there is too low for the model to grasp such detail.

Dust emission at these wavelengths is assumed to be due to fluorescence or stochastic heating caused by O and B stars with the same scale length as the old disk but with the warping ($x^d\bar{Z}$) and the scale height (h_z^d) of the dust. The dust emissivity at any point is proportional to the product of the dust density and the UV emissivity within a UV absorption length [$\propto$(dust density)$^{-1/3}$], so that

$$\rho_v^{\rm dust} = \rho_v^{\rm dust}(0) H^d H e^{-R/h_r - 2R/3h_r^d} \operatorname{sech}^{10/3}\left(\frac{|Z - x^d\bar{Z}|}{h_z^d}\right). \tag{6}$$

Note that as a product of the dust density and stellar emissivity, the emissivity of the dust falls off more rapidly in R and Z than in either of the quantities alone.

Dust-scattered starlight is neglected. However, since it is proportional to the dust density and nearly isotropic at these wavelengths, there will be an apparent correlation between scattering and emission, and some scattered light will find its way into $\rho_v^{\rm dust}$.

3.3. *The Bar Models*

Other spiral galaxies show a great variety in the shapes of their bars, as they do in many things, but some generalities have been drawn. A typical bar is straight. Its brightness along the major axis varies from roughly exponential to roughly flat and often ends abruptly. The flatter bars tend to belong to galaxies of earlier Hubble type and to be stronger, often joining directly to spiral arms or a ring (Elmegreen & Elmegreen 1985; Elmegreen et al. 1996). The outer part of a bar often has a somewhat rectangular appearance when viewed face-on (Ohta et al. 1990). See Kormendy (1977) and Sellwood & Wilkinson (1993) for general information.

The simplest bar shape is an ellipsoid. More realistically, a "generalized ellipse" has been proposed by Athanassoula et al. (1990) for the two-dimensional case of a galaxy observed face-on,

$$R_s^C = \left(\frac{|X'|}{a_x}\right)^C + \left(\frac{|Y'|}{a_y}\right)^C, \tag{7}$$

elliptical when $C = 2$, diamond- or lozenge-shaped when $C < 2$, and boxy when $C > 2$. This can be generalized to three dimensions by defining

$$R_\perp^{C_\perp} = \left(\frac{|X'|}{a_x}\right)^{C_\perp} + \left(\frac{|Y'|}{a_y}\right)^{C_\perp}, \tag{8}$$

$$R_s^{C_\parallel} = R_\perp^{C_\parallel} + \left(\frac{|Z'|}{a_z}\right)^{C_\parallel}. \tag{9}$$

The effective radius is R_s; the scale lengths are a_x, a_y, and a_z; and $C_\perp$ and $C_\parallel$ are the face-on and edge-on shape parameters. A bar may appear diamond-shaped from one vantage point and boxy from another. Athanassoula et al. (1990) and Athanassoula (1992a) found that both the ellipticity and the shape parameter of face-on galaxies varied with R, but after some unsuccessful experimentation with an R-dependent $C_\perp$ and a_x/a_y ratio, I decided to leave these parameters single valued.

The radial dependence of the bar must cover the range of flat to exponential shapes. I have tried three functions flexible enough to model this characteristic when coupled with a term that truncates them radially,

$$\text{Model S: } \rho \propto \operatorname{sech}^2(R_s), \tag{10}$$

$$\text{Model E: } \rho \propto \exp(R_s^{-n}), \tag{11}$$

and

$$\text{Model P: } \rho \propto [1 + (R_s/R_c)^n] \, . \tag{12}$$

Model S has the fewest parameters. At first, the power of the sech function was left free, but in test runs it settled so close to a value of 2.0 that I fixed it there. Giving the bar and disk the same functional Z-dependence has the advantage of allowing the direct comparison of scale heights. Model E, an exponential-to-a-power model, fitted almost as well but at the price of an extra free parameter, the power n. An n of 1.0 would give us an exponential bar, the form recommended by Stanek et al. (1997). An n of 2.0 would match the radial dependence of the best-fit model of Dwek et al. (1995). Model P, using a power law with core radius R_c, led to a distinctly inferior fit.

The bar would possibly be better fitted using a different function, rather than just a different scale length, along each axis, but I am reluctant to enter this wilderness of functional combinations without the firm guidance of theory.

To truncate the bar at radius $R_{\rm end}$, its density is multiplied by a Gaussian function with scale length $h_{\rm end}$. Both $R_{\rm end}$ and $h_{\rm end}$ are free parameters. In model S, for example, the volume emissivity of the bar is

$$\rho_v^{\rm bar} = \rho_v^{\rm bar}(0) \, \text{sech}^2 \, (R_s) \, , \quad R \le R_{\rm end} \, ; \tag{13}$$

$$\rho_v^{\rm bar} = \rho_v^{\rm bar}(0) \, \text{sech}^2 \, (R_s) e^{-(R_s - R_{\rm end})^2/h_{\rm end}^2} \, , \quad R > R_{\rm end} \, . \tag{14}$$

The bar has two more degrees of freedom: a tilt angle θ_0 (a clockwise rotation about the Z-axis from the Sun-center line) and a pitch angle (the angle between the bar's major axis and the Galactic plane).

A dust lane often runs along the leading edge of a bar, but, in the belief that masking the low-latitude sky would hide it, it is not included in my model. If a dust lane is present, we must search for it in the residuals.

4. THE FIT AND ITS RESIDUALS

The mean absolute deviations of the models, obtained using the primary mask, are given in Table 1. These are averages over the 60 fits. The MAD was the quantity optimized, but ψ and the χ^2 per degree of freedom were also calculated and are included. Ideally, the values of χ^2 and ψ would be 1.0 and 0.77, respectively, but because of the presence of the young disk, the figures of merit would not approach the ideal values even if the models of the bar and the old disk were perfect. In any case, the figures of merit are only relative and do not provide confidence limits on a model. The formal uncertainties are omitted, except in the last column, containing the weighted mean values. As expected, by all measures the J-band fit is the worst in the bar region, and the M-band fit the worst in the disk. The L band, with low extinction and very little remaining zodiacal light, provides the best fit, judging by ψ and χ^2 (the MAD cannot be used to compare different bands).

In the disk region, the figures of merit of all the models are approximately equal, indicating that the exponential part of the disk has been successfully decoupled from the inner part. In the bar region, model S has a small but consistent superiority over model E, while model P is a poor third. When the minimal mask was used, all figures of merit worsened—MAD by $\sim 10\%$ over its previous value—but the relative quality of fit among the models did not change. (They were not tabulated for this reason.)

A penalty incurred by smoothing away point sources must be discussed before contour plots of the data and model are presented. Because of the broad DIRBE beam, it

TABLE 1

QUALITY OF FIT ($R_0 = 8.5$ kpc), USING THE PRIMARY MASK

MODEL FIT PARAMETER	BAND				MEAN
	J	K	L	M	
The Disk Region[a]					
MAD_S (percent)	5.82	6.438	7.167	8.407	6.790 ± 0.022
MAD_E (percent)	5.871	6.465	7.226	8.451	6.815 ± 0.032
MAD_P (percent)	5.938	6.485	7.164	8.223	6.791 ± 0.029
ψ_S	1.199	1.182	1.106	1.743	1.209 ± 0.006
ψ_E	1.209	1.180	1.114	1.749	1.213 ± 0.005
ψ_P	1.223	1.190	1.100	1.676	1.207 ± 0.006
χ_S^2	4.97	3.61	2.849	6.07	3.805 ± 0.039
χ_E^2	4.74	3.67	2.887	6.09	3.808 ± 0.035
χ_P^2	4.67	3.70	2.881	5.67	3.768 ± 0.034
The Bar Region[b]					
MAD_S (percent)	7.53	4.356	3.856	4.378	4.197 ± 0.027
MAD_E (percent)	7.52	4.683	3.903	4.388	4.304 ± 0.024
MAD_P (percent)	8.70	4.744	4.247	5.192	4.716 ± 0.028
ψ_S	2.204	1.312	0.958	1.214	1.149 ± 0.007
ψ_E	2.249	1.420	0.975	1.233	1.190 ± 0.007
ψ_P	2.522	1.408	1.030	1.402	1.262 ± 0.010
χ_S^2	16.9	4.91	2.54	3.53	3.69 ± 0.05
χ_E^2	16.1	5.54	2.61	3.70	3.93 ± 0.06
χ_P^2	20.8	21.7	19.1	22.2	20.8 ± 1.3

NOTE.—The mean absolute fractional deviation, MAD, is the quantity that was minimized.

[a] Weights are 0.182, 0.364, 0.364, and 0.091 for the J, K, L, and M bands, respectively.

[b] Weights are 0.014, 0.282, 0.423, and 0.282 for the J, K, L, and M bands, respectively.

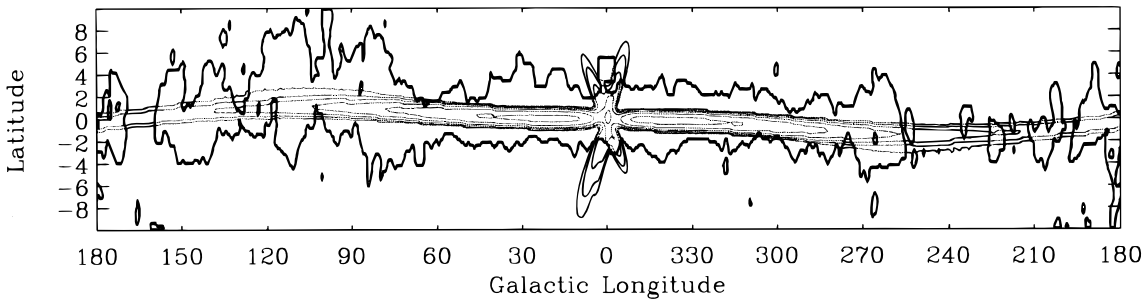

FIG. 2.—Fractional increase in surface brightness (model S) when the point-source removal process is not applied. The outermost contour level is at 0.25%. Each level inward is a factor of 2 higher. The thick contour represents the primary rejection mask.

is difficult to distinguish between nearby stars and pointlike but extended distant sources, such as those on the brightness crest of the inner Galaxy. As a consequence, the brightness crest is rounded off. The effect of this on the old disk can be gauged by applying the same procedure to the modeled *L*-band surface brightness map. In Figure 2 we have the difference between the unsmoothed and smoothed maps from model S as a fraction of the unsmoothed map's surface brightness. The effect is greatest in a narrow strip approximately 2° wide, the size of the minimal mask. An X appears where the corners of the bulge have been eroded, but it is very faint and fills only a small part of the bulge region. This figure tells us that if data and model are to be compared over the whole sky and not just over the nonmasked area, both must be either smoothed or unsmoothed (it also reminds us that a boxy bulge may appear X-shaped if a nonboxy model is subtracted from it).

Figure 3 compares the smoothed DIRBE *L*-band map to the smoothed map made using model S, with the primary rejection mask overlaid. In this two-dimensional projection, models E and S are very similar. In the nonmasked region, the agreement between data and model is excellent. The major discrepancies occur in the direction of the local spiral arm or spur in Cygnus and toward the molecular clouds in Ophiuchus, Orion, and Taurus.

While Figure 3 tells us how well model and data agree, the disagreements are best examined by focusing on the residuals. In Figures 4, 5, 6, and 7, the smoothed modeled surface brightness, using model S and the primary mask, has been subtracted in stages from the smoothed DIRBE *J* through *M* sky maps. In the *J* map, the final residuals are predominantly negative. There is more extinction, especially at positive latitudes, than the model predicts. Proceeding from the *J* through the *K*, *L*, and *M* bands, the extinction lessens and the negative residue approaches zero. It does not reach zero, however, suggesting a flaw in the model, perhaps in its treatment of the dust layer.

There is much information in these plots of residuals, but as that information does not include distances, the plots should be interpreted with care. Most prominent in the residuals is a bright nucleus roughly 2° (or 300 pc at a distance of 8.5 kpc) in diameter. This becomes brighter and morphologically simpler as the observing wavelength increases and probably does occupy the center of the Galaxy, a unique environment in which the model is certainly inadequate (see, for example, Morris & Serabyn 1996). There is also a bright narrow ridge in the inner Galaxy along the Galactic midplane, probably created by stars associated with the young disk, red supergiants in particular. The ridge is brighter at positive longitudes and

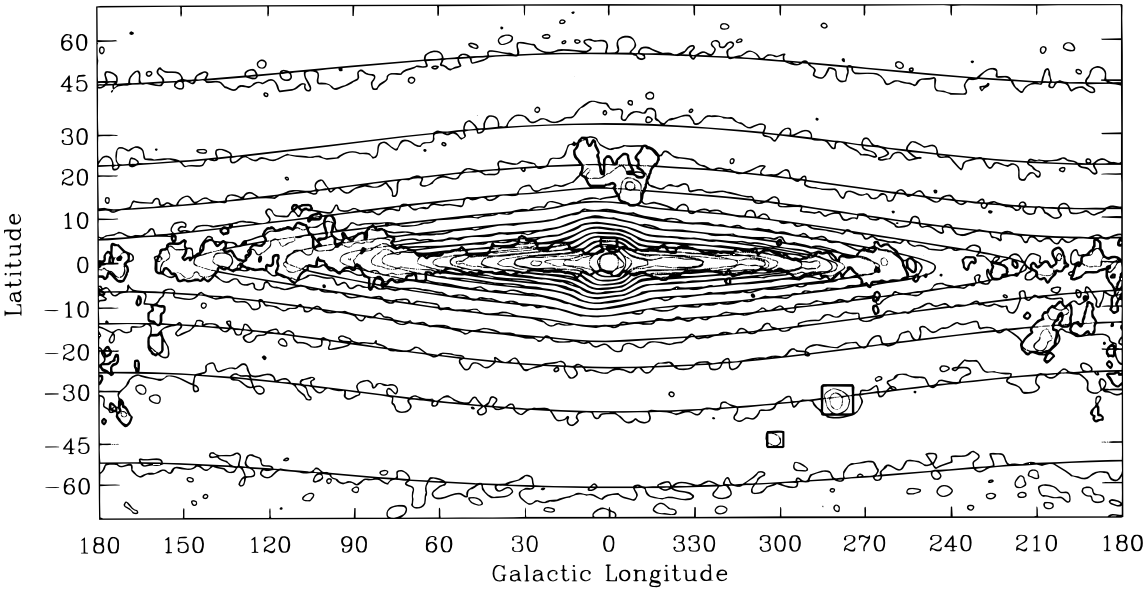

FIG. 3.—*L*-band (3.5 μm) DIRBE and model S (*smooth isophotes*) surface brightness over the full sky. The area within the dark contour was excluded when the model was fitted to the data. The surface brightness due to point sources, as calculated by the model, was added to both. The contour levels are 0.09, 0.13, 0.18, 0.26, 0.52, 0.73, 1.04, 1.47, 2.08, 2.94, 4.17, 5.90, and 8.36 MJy sr^{-1}.

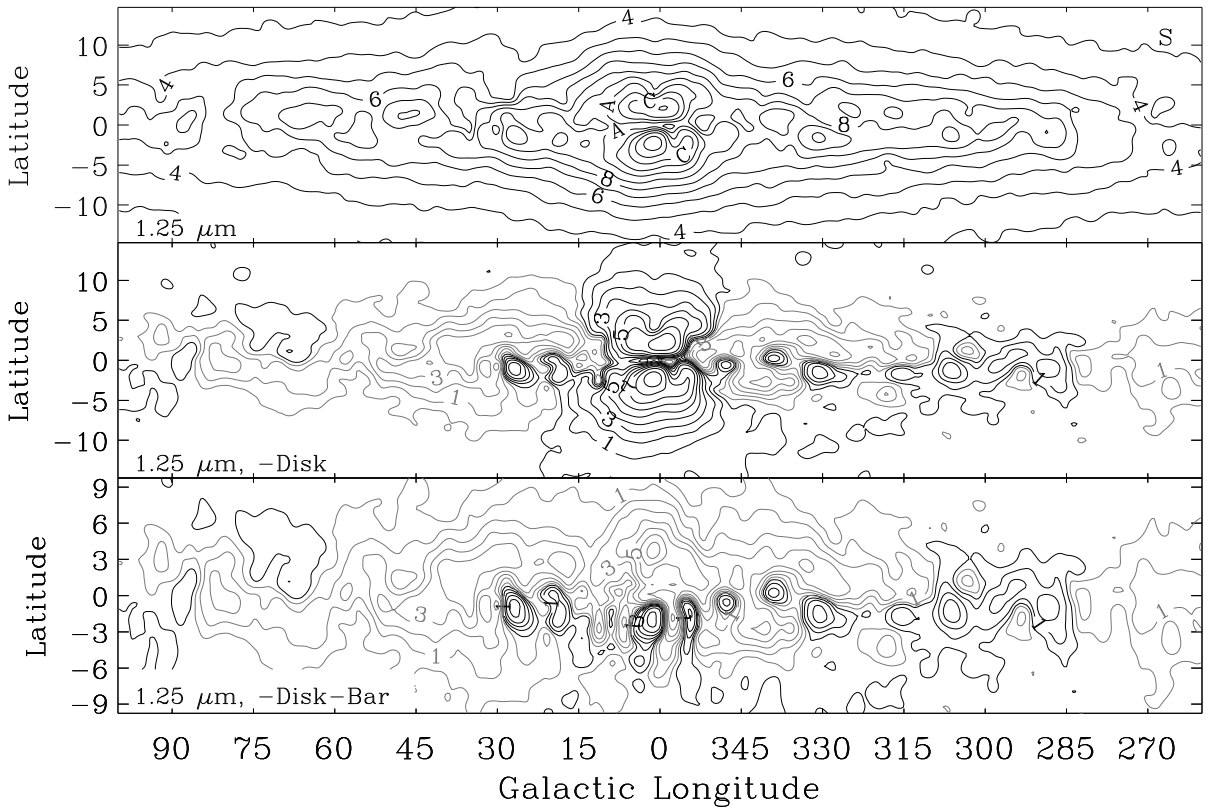

FIG. 4.—*J*-band (1.25 μm) map (*top*), and *J*-band map after the modeled disk (*middle*) and the modeled disk and bar (*bottom*) are subtracted. The gray contours represent $I_\nu < 0$. Contour levels are numbered hexadecimally, starting at 0. The levels (in MJy sr^{-1}) are 0.06, 0.21, 0.39, 0.62, 0.91, 1.27, 1.73, 2.31, 3.04, 3.96, and 5.11 (*top*); $\pm$ 0.08, 0.30, 0.59, 1.00, 1.54, 2.30, 3.32, 4.73, 6.65, and 9.28 (*middle*); and $\pm$ 0.07, 0.25, 0.49, 0.80, 1.21, 1.75, 1.75, 2.45, and 3.38 (*bottom*).

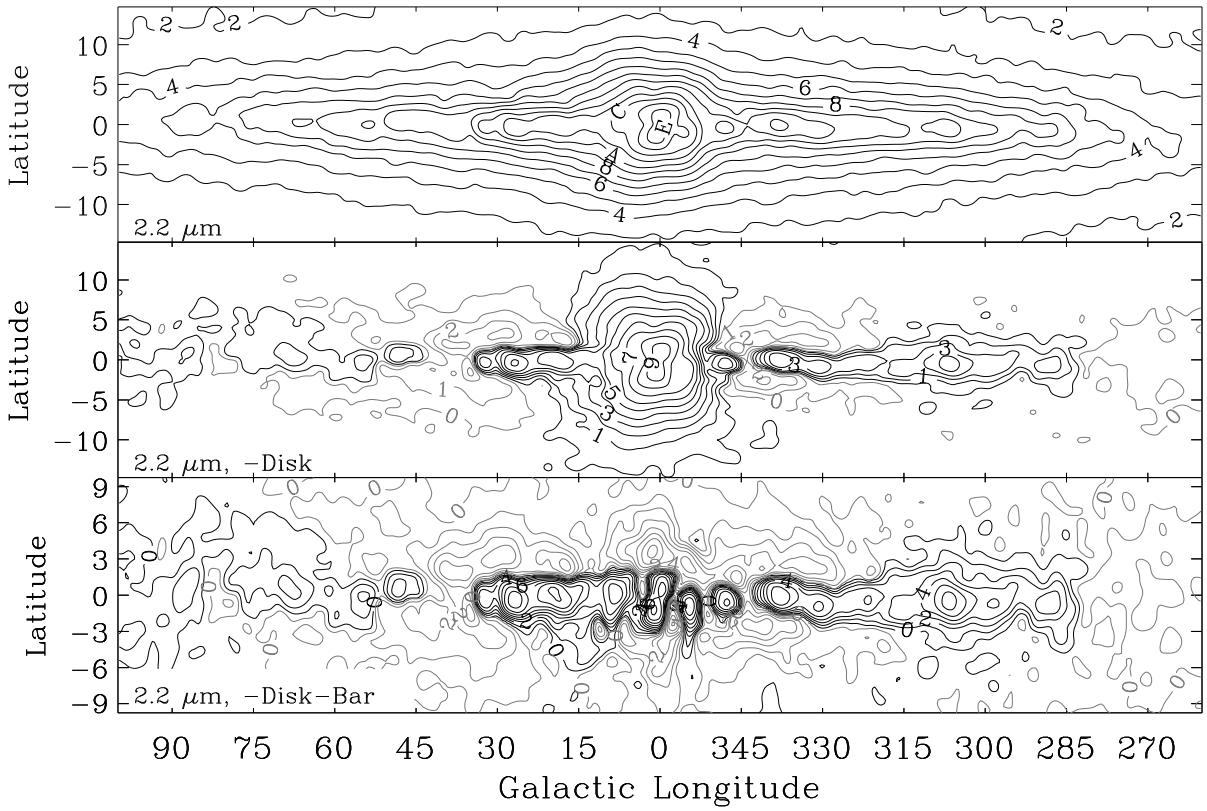

FIG. 5.—*K*-band (2.2 μm) map (*top*), and *K*-band map after the modeled disk (*middle*) and the modeled disk and bar (*bottom*) are subtracted. The gray contours represent $I_\nu < 0$. Contour levels are numbered hexadecimally, starting at 0. The levels (in MJy sr^{-1}) are 0.07, 0.23, 0.44, 0.71, 1.06, 1.51, 2.10, 2.84, 3.81, 5.05, 6.65, 8.71, 11.4, and 14.8 (*top*); $\pm$ 0.09, 0.34, 0.68, 01.17, 1.86, 2.83, 4.20, 6.14, 8.88, and 12.7 (*middle*); and $\pm$ 0.07, 0.23, 0.44, 0.71, 1.06, 1.50, 2.08, 2.82, and 3.78 (*bottom*).

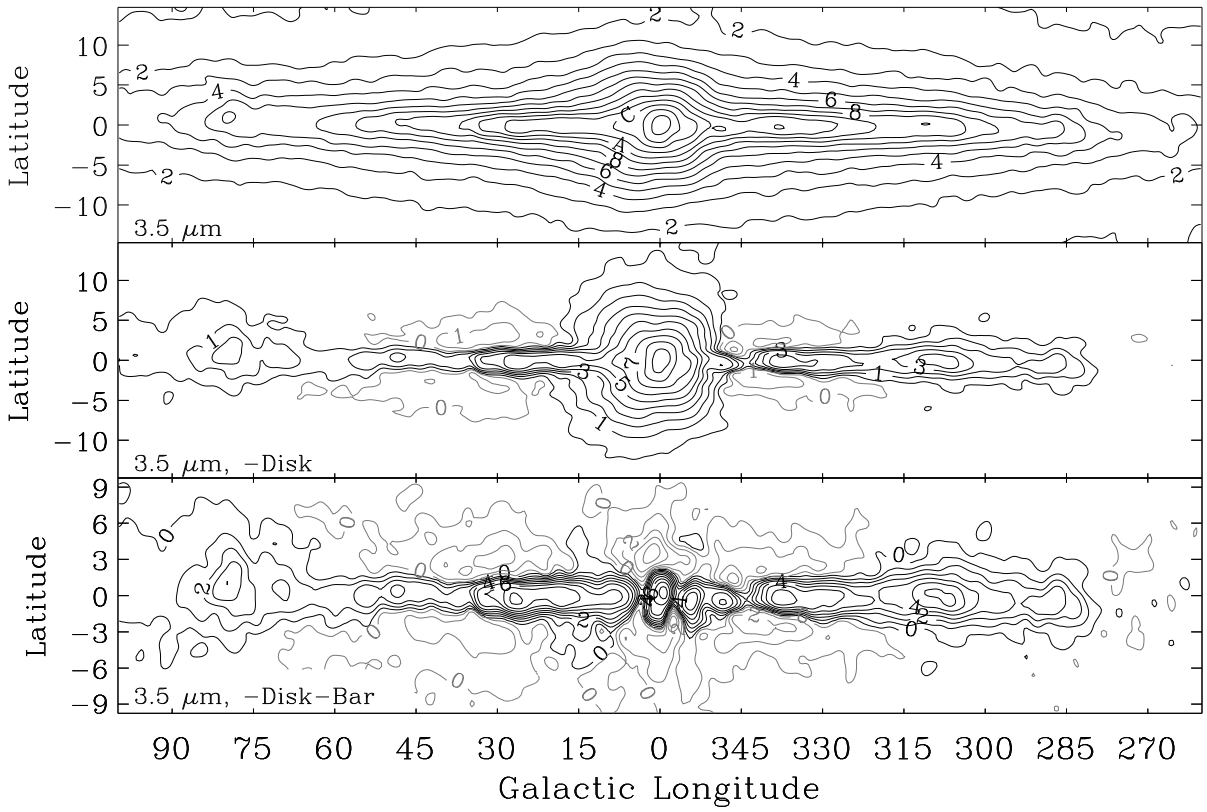

FIG. 6.—*L*-band (3.5 μm) map (*top*), and *L*-band map after the modeled disk (*middle*) and the modeled disk and bar (*bottom*) are subtracted. The gray contours represent $I_\nu < 0$. Contour levels are numbered hexadecimally, starting at 0. The levels (in MJy sr^{-1}) are 0.06, 0.22, 0.41, 0.66, 0.97, 1.37, 1.87, 2.52, 3.33, 4.37, 5.69, 7.36, 9.49, 12.2, and 15.6 (*top*); $\pm$ 0.09, 0.31, 0.62, 1.05, 1.64, 2.46, 3.59, 5.14, 7.30, and 10.3 (*middle*); and $\pm$ 0.06, 0.21, 0.40, 0.64, 0.94, 1.33, 1.82, 2.43, and 3.21 (*bottom*).

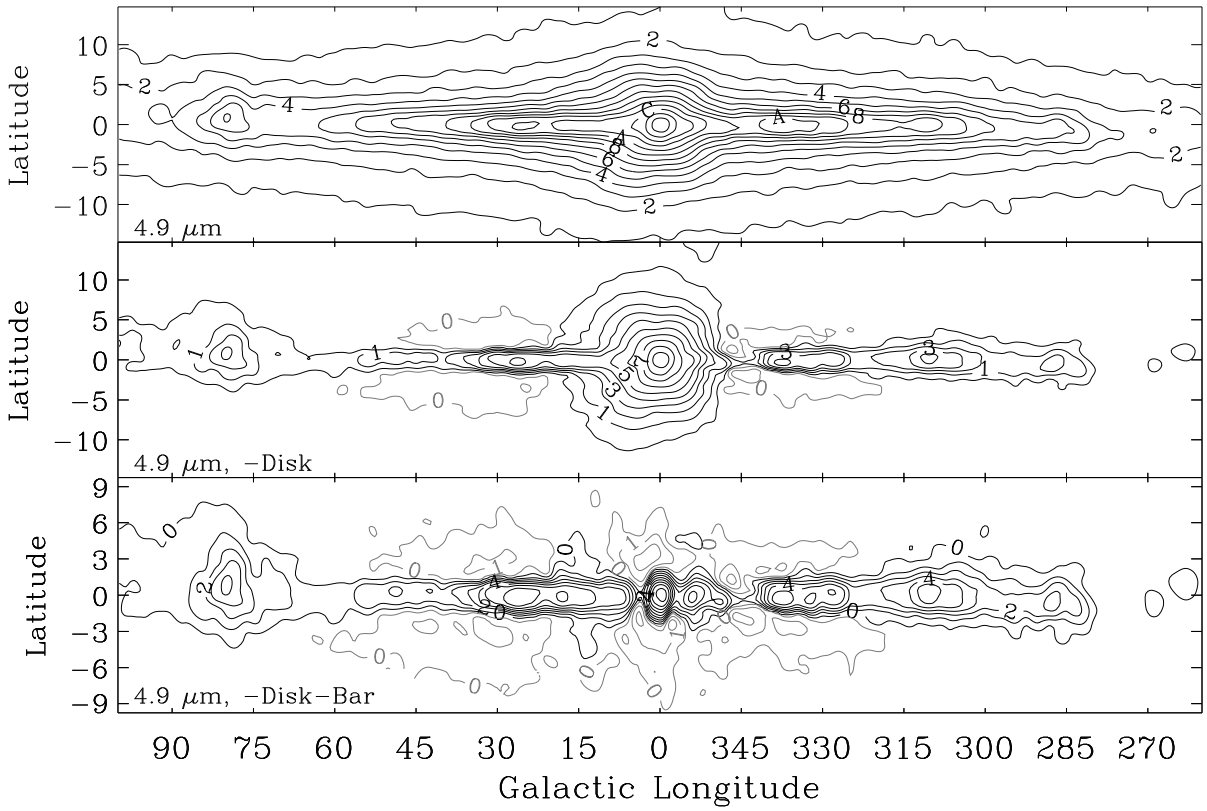

FIG. 7.—*M*-band (4.9 μm) map (*top*), and *M*-band map after the modeled disk (*middle*) and the modeled disk and bar (*bottom*) subtracted. The gray contours represent $I_\nu < 0$. Contour levels are numbered hexadecimally, starting at 0. The levels (in MJy sr^{-1}) are 0.06, 0.19, 0.35, 0.55, 0.80, 1.11, 1.50, 1.97, 2.56, 3.29, 4.19, 5.30, 6.68, 8.38, and 10.5 (*top*); $\pm$ 0.08, 0.26, 0.51, 0.84, 1.28, 1.87, 2.64, 3.66, 5.02, and 6.82 (*middle*); and $\pm$ 0.06, 0.19, 0.36, 0.84, 1.17, 1.57, 2.08, and 2.71 (*bottom*).

fainter and partially broken at negative longitudes. It is tempting to link this asymmetric feature to the bar. Hammersley et al. (1994) identified peaks in the DIRBE K-band surface brightness at $l = 21°$ and 27° as probably originating in star-forming regions at the near end of a bar, which would need to be long (3.7–4 kpc) and viewed almost broadside (at an angle of $75° \pm 5°$). Calbet et al. (1996) developed this idea further. Since the oblong boxy bulge seen in the DIRBE maps is much too narrow to be explained by such a bar, the bar must be very thin in Z and exist in addition to what they refer to as the "thin bulge." It appears, however, that the "thin bulge" is actually a strong bar stretching more than 3 kpc from the Galactic center, and two bars of roughly the same length are not observed in other spiral galaxies. These peaks of brightness noted by Hammersley et al. (1994) do occur in my model-subtracted maps. They appear even brighter and extend further in l in the L and M bands. Yet I prefer to locate these peaks on an arc or arm trailing the bar's near end or on a bright segment of a bar-circling ring. I agree with Calbet et al. (1996) that extinction caused by a dust lane could cause the brightness ridge to appear fainter in the fourth Galactic quadrant. In the first quadrant, we probably see the trailing edge of the near end of the bar and in the fourth the leading edge of the far end. The dips in the surface brightness for $-12° > l > 0°$ could well be caused by dust within or at the leading edge of the bar. At more negative longitudes I believe we must search for other explanations.

When the minimal mask is used, there is no great change in any one parameter. Extinction toward the inner Galaxy decreases slightly, and the residuals acquire a small shift toward the negative, as can be seen in Figure 8, which shows the final L-band residuals of model S. The surface brightness toward the Galactic center and the brightness crest to either side simply cannot be accounted for by the model. Using the minimal mask probably gains us nothing but the greater opportunity to be biased by features extraneous to the bar and old disk. Figure 8 is the only figure presented that involves the minimal mask, but the values of the model parameters will be tabulated for both masks (see Tables 2 and 3, discussed in § 5), to give some idea of the possible bias entailed.

Now we move to the unsmoothed maps. Figure 9 (Plate 6) displays pseudocolor images from the J, K, and L bands before and after model subtraction. Translating from color to surface brightness may be difficult because of the unusual color table, which is better at displaying shape and detail, but that information is available in the contour plots already discussed. Figure 10 (Plate 7) combines the J, K, and L residual maps in a three-color image. The aforementioned Galactic nucleus and brightness ridge are evident. Extended white patches mark the locations of low-extinction windows. Appearing as pink or red are directions in which the extinction is unusually heavy or there is significant emission by dust or by luminous dust-shrouded stars. There are spurs of heavier extinction reaching upward from $l \approx 0°$ and $l \approx \pm 25°$. These have counterparts in far-infrared image presented in Paper I (Fig. 2*b* of that paper) and in maps of CO emission (see Fig. 6 of Dame et al. 1987), which is strongly correlated with dust density.

Figure 11 (Plate 8) presents the same composite, before and after model subtraction, on a logarithmic brightness scale so the bulge does not overwhelm the disk. The fact that the disk and the bulge are morphologically identical at the three wavelengths and have been scaled to the same emissivity causes the three colors to sum to a gray haze where the column density of the dust is low; the residuals actually appear brighter than the original DIRBE image.

5. DISCUSSION OF THE MODELS

5.1. *The Tabulated Parameter Values*

The values of the parameters of the three models were normally distributed. Their means and the standard deviations of the means are listed in Tables 2 and 3. Of course, the standard deviations tell us more about the models' consistency than about their validity. Comparison of models S and E, and of the results obtained using the primary and the minimal masks, probably provide a better idea of the true uncertainties. In going from the primary to the minimal mask, the major change is a decrease in extinction.

It might have been misleading to include the coefficients c_i of the cubic polynomial that describes the amplitude of the warp, since the coefficients are not independent. Instead, the shape of the warp is shown graphically in Figure 12. As noted in Paper I, the orientation and magnitude of the warping is consistent with that of the H I layer, the shape of which, however, is not known very precisely for $R < 12$ kpc.

In all models, the deletion distances $D_\nu \approx 470$, 520, 560, and 560 pc for bands J through M, respectively, and the respective offsets in surface brightness δ_ν are 84, 64, 31, and 14 kJy sr^{-1}. These numbers include the extragalactic background but are also functions of the data reduction process, so one should not read too much into them.

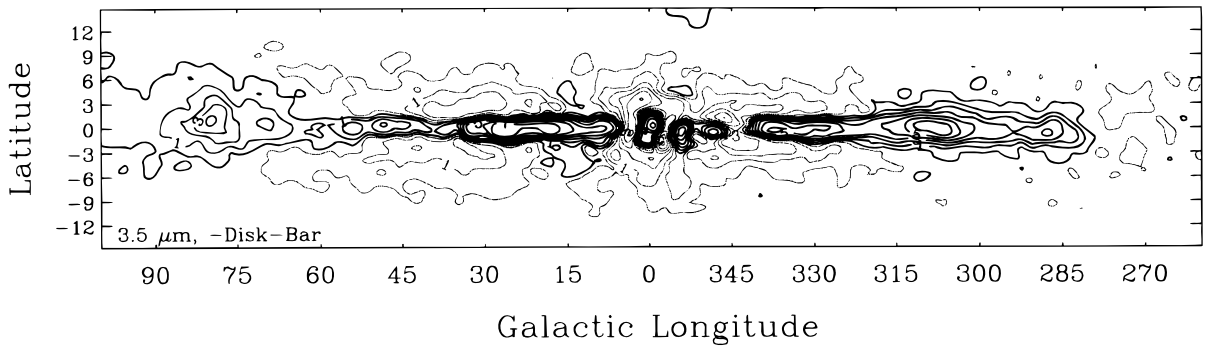

FIG. 8.—L-band (3.5 μm) map after the modeled disk and bar are subtracted. The minimal mask was used in fitting the model. The gray contours represent $I_\nu < 0$. Contour levels are numbered hexadecimally, starting at 0. The contour levels are $\pm$ 0.06, 0.21, 0.40, 0.64, 0.94, 1.33, 1.82, 2.43, and 3.21 MJy sr^{-1}.

TABLE 2

PARAMETER VALUES ($R_0 = 8.5$ kpc), USING THE PRIMARY MASK

Parameter	Model S	Model E	Model P
Distance to Galactic plane Z_0 (pc)	16.46 ± 0.18	16.60 ± 0.15	15.95 ± 0.14
Bar tilt angle θ_0 (deg)	13.79 ± 0.09	9.52 ± 0.12	13.18 ± 0.13
Disk scale length h_r (kpc)	2.6045 ± 0.0033	2.6030 ± 0.0030	2.567 ± 0.0030
Disk scale height h_z (kpc)	0.3457 ± 0.0008	0.3519 ± 0.0011	0.3467 ± 0.0010
Disk radius R_{max} (kpc)	12.18 ± 0.06	12.47 ± 0.05	12.43 ± 0.07
Warp line of nodes ϕ_W (deg)	0.44 ± 0.09	0.79 ± 0.09	-0.08 ± 0.11
Disk $\rho_J(0)$ (MJy sr^{-1} kpc^{-1})	8.157 ± 0.024	8.133 ± 0.032	8.786 ± 0.032
Disk $\rho_K(0)$ (MJy sr^{-1} kpc^{-1})	6.648 ± 0.022	6.659 ± 0.024	6.970 ± 0.023
Disk $\rho_L(0)$ (MJy sr^{-1} kpc^{-1})	3.511 ± 0.009	3.449 ± 0.012	3.614 ± 0.012
Disk $\rho_M(0)$ (MJy sr^{-1} kpc^{-1})	1.782 ± 0.006	1.738 ± 0.005	1.802 ± 0.006
Disk-hole radius O_R (kpc)	2.973 ± 0.022	2.956 ± 0.020	3.323 ± 0.018
Disk-hole power O_N	1.711 ± 0.016	1.595 ± 0.017	1.593 ± 0.023
Hole axis ratio ε	0.8554 ± 0.0042	0.904 ± 0.005	0.939 ± 0.007
Bar pitch angle (deg)	-0.023 ± 0.027	0.046 ± 0.018	-0.021 ± 0.025
Bar X scale length a_x (kpc)	1.696 ± 0.007	1.888 ± 0.010	1.810 ± 0.009
Bar Y scale length a_y (kpc)	0.6426 ± 0.0020	0.6561 ± 0.0035	0.6450 ± 0.0038
Bar Z scale length a_z (kpc)	0.4425 ± 0.0008	0.4301 ± 0.0020	0.4324 ± 0.0031
Bar cutoff radius R_{end} (kpc)	3.128 ± 0.014	3.574 ± 0.021	2.713 ± 0.015
Bar cutoff scale length h_{end} (kpc)	0.461 ± 0.005	0.562 ± 0.008	0.882 ± 0.006
Bar face-on Shape $C_\perp$	1.574 ± 0.014	1.609 ± 0.020	1.651 ± 0.022
Bar edge-on Shape $C_\parallel$	3.501 ± 0.016	3.493 ± 0.025	3.016 ± 0.023
Bar $\rho_J(0)$ (MJy sr^{-1} kpc^{-1})	10.52 ± 0.07	10.29 ± 0.08	11.67 ± 0.06
Bar $\rho_K(0)$ (MJy sr^{-1} kpc^{-1})	8.817 ± 0.038	8.700 ± 0.048	9.40 ± 0.05
Bar $\rho_L(0)$ (MJy sr^{-1} kpc^{-1})	4.538 ± 0.017	4.452 ± 0.022	4.880 ± 0.024
Bar $\rho_M(0)$ (MJy sr^{-1} kpc^{-1})	2.255 ± 0.009	2.203 ± 0.010	2.388 ± 0.015
Bar power n	...	1.4439 ± 0.0049	5.044 ± 0.031
Bar core radius R_c (kpc)	...	...	1.231 ± 0.007
Dust scale length h_r^d (kpc)	3.066 ± 0.019	3.348 ± 0.021	3.425 ± 0.023
Dust scale height h_z^d (kpc)	0.1520 ± 0.0008	0.1474 ± 0.0009	0.1465 ± 0.0007
Dust warp factor x^d	1.782 ± 0.009	1.755 ± 0.011	1.754 ± 0.009
Local extinction A_J (J mag kpc^{-1})	0.1144 ± 0.0020	0.1451 ± 0.0027	0.1528 ± 0.0028
Extinction index α	1.787 ± 0.009	1.762 ± 0.010	1.798 ± 0.010
Dust hole radius O_R^d (kpc)	2.615 ± 0.019	2.253 ± 0.017	2.025 ± 0.025
Dust hole power O_N^d	2.150 ± 0.022	2.107 ± 0.023	2.463 ± 0.020
Dust $\rho_J(0)$ (MJy sr^{-1} kpc^{-1})	4.642 ± 0.023	4.659 ± 0.025	4.819 ± 0.029
Dust $\rho_K(0)$ (MJy sr^{-1} kpc^{-1})	1.152 ± 0.007	1.225 ± 0.008	1.158 ± 0.010
Dust $\rho_L(0)$ (MJy sr^{-1} kpc^{-1})	2.180 ± 0.014	2.294 ± 0.018	2.437 ± 0.017
Dust $\rho_M(0)$ (MJy sr^{-1} kpc^{-1})	3.236 ± 0.021	3.142 ± 0.021	3.559 ± 0.023

The tilt angle of the bar, θ_0, is grouped with Z_0. To place it with the bar parameters would be chauvinistic.

Since they differ only in bar modeling, it is not surprising that the models agree on most disk and dust-layer parameters. The plausibility of the parameters describing the stellar disk was discussed in Paper I, but the parameters describing the dust layer require further discussion.

5.2. *Comparison to Paper I, and a Correction*

Paper I contained two errors, both concerning the dust layer. One occurs only in the values of A_J found in Tables 2 and 3 of that paper. They have been erroneously multiplied by a factor of 2. For example, for $R_0 = 8.5$ kpc, A_J should read "0.213" mag kpc^{-1}. This error is found only in the

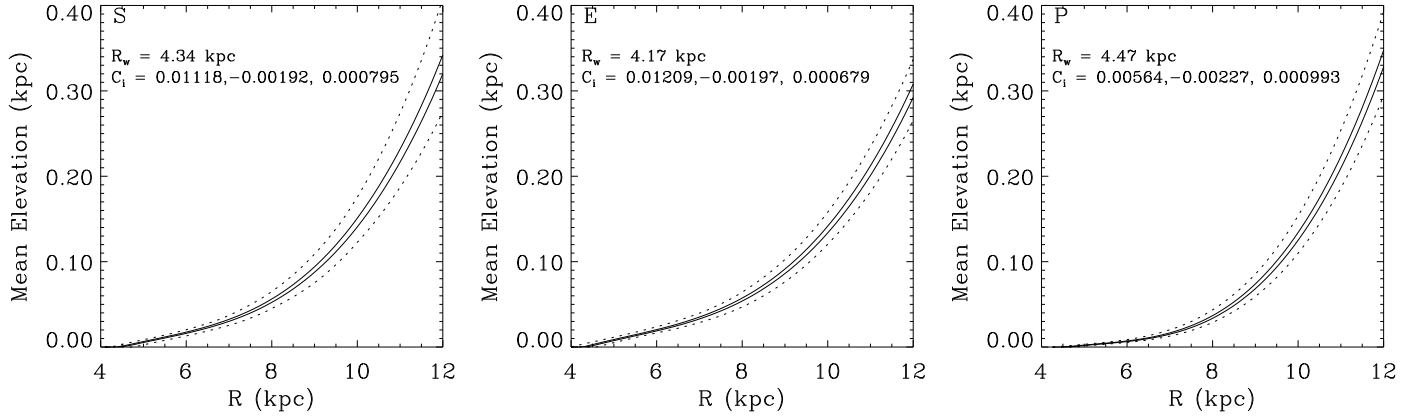

FIG. 12.—Warping of the disk, according to the three models. The dashed curves enclose 90% of the fits made. The solid curves enclose the 95% confidence limit on the mean elevation. The coefficients are those of a cubic polynomial in $R - R_w$.

TABLE 3

PARAMETER VALUES ($R_0 = 8.5$ kpc), USING THE MINIMAL MASK

Parameter	Model S	Model E	Model P
Distance to Galactic plane Z_0 (pc)	16.12 ± 0.19	16.50 ± 0.19	15.66 ± 0.14
Bar tilt angle θ_0 (deg)	13.98 ± 0.14	9.84 ± 0.12	13.51 ± 0.13
Disk scale length h_r (kpc)	2.6009 ± 0.0040	2.601 ± 0.007	2.567 ± 0.006
Disk scale height h_z (kpc)	0.3420 ± 0.0008	0.3466 ± 0.0011	0.3440 ± 0.0012
Disk radius $R_{\max}$ (kpc)	12.35 ± 0.06	12.45 ± 0.07	12.52 ± 0.08
Warp line of nodes ϕ_W (deg)	0.40 ± 0.11	0.83 ± 0.10	-0.07 ± 0.12
Disk $\rho_J(0)$ (MJy sr^{-1} kpc^{-1})	8.115 ± 0.036	8.141 ± 0.043	8.725 ± 0.046
Disk $\rho_K(0)$ (MJy sr^{-1} kpc^{-1})	6.707 ± 0.029	6.740 ± 0.026	7.000 ± 0.036
Disk $\rho_L(0)$ (MJy sr^{-1} kpc^{-1})	3.539 ± 0.013	3.478 ± 0.013	3.637 ± 0.014
Disk $\rho_M(0)$ (MJy sr^{-1} kpc^{-1})	1.759 ± 0.008	1.724 ± 0.008	1.796 ± 0.010
Disk-hole radius O_R (kpc)	2.912 ± 0.029	2.910 ± 0.020	3.294 ± 0.025
Disk-hole power O_N	1.705 ± 0.020	1.572 ± 0.015	1.585 ± 0.017
Hole axis ratio ε	0.822 ± 0.022	0.905 ± 0.021	0.910 ± 0.014
Bar pitch angle (deg)	-0.05 ± 0.08	0.07 ± 0.09	0.02 ± 0.08
Bar X scale length a_x (kpc)	1.686 ± 0.011	1.878 ± 0.011	1.806 ± 0.010
Bar Y scale length a_y (kpc)	0.6429 ± 0.0032	0.6512 ± 0.0036	0.6418 ± 0.0028
Bar Z scale length a_z (kpc)	0.4420 ± 0.0013	0.4302 ± 0.0018	0.4313 ± 0.0022
Bar cutoff radius $R_{\rm end}$ (kpc)	3.139 ± 0.021	3.542 ± 0.019	2.725 ± 0.013
Bar cutoff scale length $h_{\rm end}$ (kpc)	0.469 ± 0.020	0.545 ± 0.019	0.875 ± 0.013
Bar face-on shape $C_\perp$	1.588 ± 0.017	1.597 ± 0.022	1.655 ± 0.019
Bar edge-on shape $C_\parallel$	3.466 ± 0.028	3.418 ± 0.022	2.976 ± 0.023
Bar $\rho_J(0)$ (MJy sr^{-1} kpc^{-1})	10.42 ± 0.14	10.36 ± 0.09	11.77 ± 0.08
Bar $\rho_K(0)$ (MJy sr^{-1} kpc^{-1})	8.769 ± 0.045	8.707 ± 0.044	9.40 ± 0.06
Bar $\rho_L(0)$ (MJy sr^{-1} kpc^{-1})	4.545 ± 0.024	4.465 ± 0.020	4.878 ± 0.021
Bar $\rho_M(0)$ (MJy sr^{-1} kpc^{-1})	2.241 ± 0.015	2.180 ± 0.015	2.387 ± 0.013
Bar power n	...	1.438 ± 0.005	5.004 ± 0.031
Bar core radius R_c (kpc)	...	...	1.224 ± 0.005
Dust scale length h_r^d (kpc)	3.020 ± 0.029	3.320 ± 0.026	3.376 ± 0.021
Dust scale height h_z^d (pc)	0.205 ± 0.006	0.2019 ± 0.0048	0.182 ± 0.006
Dust warp factor x^d	1.811 ± 0.019	1.765 ± 0.014	1.749 ± 0.012
Local extinction A_J (J mag kpc^{-1})	0.0898 ± 0.0033	0.1116 ± 0.0038	0.1236 ± 0.0039
Extinction index α	1.987 ± 0.023	2.011 ± 0.024	1.979 ± 0.020
Dust hole radius O_R^d (kpc)	2.684 ± 0.032	2.222 ± 0.020	2.051 ± 0.026
Dust hole power O_N^d	2.182 ± 0.023	2.116 ± 0.012	2.466 ± 0.020
Dust $\rho_J(0)$ (MJy sr^{-1} kpc^{-1})	4.681 ± 0.028	4.699 ± 0.034	4.795 ± 0.036
Dust $\rho_K(0)$ (MJy sr^{-1} kpc^{-1})	1.146 ± 0.008	1.229 ± 0.008	1.145 ± 0.010
Dust $\rho_L(0)$ (MJy sr^{-1} kpc^{-1})	2.196 ± 0.018	2.320 ± 0.024	2.455 ± 0.019
Dust $\rho_M(0)$ (MJy sr^{-1} kpc^{-1})	3.185 ± 0.031	3.139 ± 0.025	3.559 ± 0.026

tables. It is also moot because of an error in the software. The extinction in the different bands was to be related by the law of Rieke & Lebofsky (1985), which has a power-law index $\alpha = 1.765$ in bands J through M. In the modeling program, this index became 1.33, which affected other parameters of the dust-layer model. What should those parameters have been? Using model S without a disk hole and minimizing ψ, as in Paper I, rather than the MAD, led to stellar disk parameters almost identical to those in Paper I. For $R_0 = 8.5$ kpc, $h_r = 2.63$ kpc, $h_z = 0.336$ kpc, $R_{\max} = 12.03$ kpc, $Z_0 = 15.60$ pc, and so on. The dust layer parameters did change: $h_r^d = 3.13$ kpc, $h_z^d = 0.20$ kpc, $A_J = 0.132$ mag kpc^{-1}, and $\alpha = 1.79$. Of these new numbers, the newer, smaller value of A_J is closer to the expected value. The value of h_z^d is larger than expected, even when the inner Galaxy is included and h_z^d drops to 0.15 kpc, but here my expectations were probably at fault. A review of H I in the Galaxy by Dickey & Lockman (1990) models the vertical structure of the H I layer, $0.4\,R_0 < R < R_0$, using the sum of two Gaussian terms and one exponential. This is shown in Figure 13, along with the profile derived from model S, $\rho^{\rm dust} \propto \mathrm{sech}^2(Z/0.152\ \mathrm{kpc})$. For $Z < 200$ pc, the two curves almost coincide, but at higher elevations the density falls off more rapidly in my model. If the H I and dust layers have the same vertical structure and Dickey & Lockman (1990) have accurately described it, then the model underestimates the extinction at higher elevations. Could this have caused the areas of negative residuals that lie a few degrees off the brightness crest of the inner Galaxy? Substituting the Z dependence of the H I for the $\mathrm{sech}^2(Z)$ term in the dust layer produced as good a fit to the data, with the parameter values almost unchanged, but did not improve the residuals. It is still possible, though, that a more sophisticated treatment of the dust layer is called for.

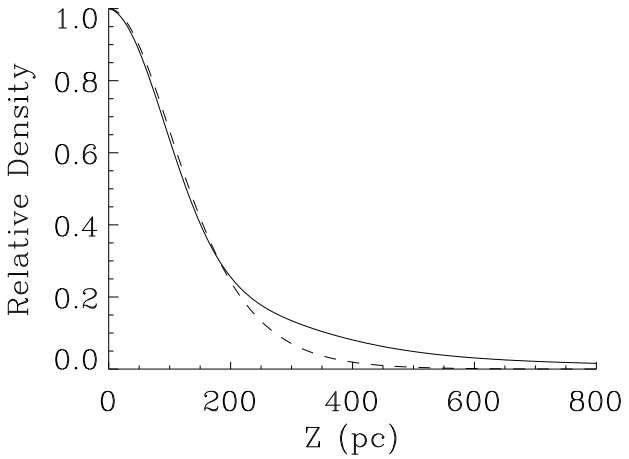

FIG. 13.—Vertical density distributions of neutral hydrogen and diffuse dust. The solid curve is the dust density from model S, with $R_0 = 8.5$ kpc. The dashed curve is the H I density from Dickey & Lockman (1990).

One other change since Paper I is the switch from a dust density $\propto 0.5$ sech (R) to a simple exponential. This did not make a significant difference.

In all three models, the stellar disk parameters are consistent with those of Paper I, with the exception of Z_0. In all models, the distance of the Sun from the Galactic plane rises several tenths of a parsec to a parsec when the disk is allowed a central hole.

5.3. *The Luminosity of the Dust Layer*

The central emissivities of the dust layer, $\rho_\nu^{\rm dust}(0)$, are of the same order of magnitude as those of the disk and bar, but then there is no dust in the center of the Galaxy, according to the model, and at larger R the more rapid radial decrease in the emissivity of the dust causes it to drop well below the stellar emissivity of even the M band. According to model S, if we observed the Galaxy face-on, we would see the ratio of L-band dust to disk surface brightness peak at a value of 4.1% at $R = 2.74$ kpc. At R_0, the ratio would be only 0.5%. In the M band, these ratios would be 12% and 1.5%, respectively. These numbers would undoubtedly be higher if dust associated with the masked-out molecular clouds were included, but near-infrared dust emission would still be a minor component of the Galaxy's luminosity. The radius of the dust layer's hole is smaller than that of the disk. The presence of the 3 kpc molecular cloud ring and possibly a stellar ring, both absent in the model, and the model's lack of sensitivity to dust in the background of most of the stellar emission suggest that this result be treated with caution.

5.4. *The Disk and its Hole*

The parameters that describe the exponential part of the disk ($R > \sim 5$ kpc) are almost unchanged from Paper I. The radius of the Galactic disk is still a mere 12 kpc. Robin, Crézé, & Mohan (1996) placed the edge of the disk 5.5 kpc from the solar circle, or $R \approx 14$ kpc. Their distance measure, based on $V-I$ color, may be wrong or, as previously discussed, one or more of the basic assumptions of my model may break down in the outer Galaxy.

The central hole in the disk appears in all three models. Forcing the disk to be exponential all the way to its center results in poor fits in all models. The value of the MAD in the bar region rises from 4.2% to 5.4%, and χ^2 increases by a factor of 5. The exponential part of the disk does not change appreciably. It becomes slightly thinner—$h_r/h_z \approx$ 7.8 instead of 7.5.

The axis ratio of the disk hole is near the middle of the range of 0.7 to 1.0 that Buta (1986) gives for stellar rings circumscribing bars. Strongly barred spiral galaxies that do not have rings are usually of grand design, with one arm trailing from each end of the bar. When ringed, they are usually multiarmed, with arms beginning at points on the ring that seem unrelated to the bar's orientation. The best evidence to date suggests that the Galaxy is of the second type (Valée 1995). I suspect it is also ringed.

5.5. *The Bar and the Disk Hole*

In all three models, the bar ends at the inner edge of the Galaxy's molecular cloud ring, at $R \approx 3.5$ kpc, in agreement with observations of other spiral galaxies and with simulations that show that a strong rotating bar sweeps up the gas and dust in its vicinity (Athanassoula 1992b). There seems to be a current consensus that rings form at the inner second harmonic resonance (Schwartz 1984), just inside the corotation radius, beyond which bars cannot extend (Contopoulos et al. 1989).

Figure 14 shows the face-on surface brightness predicted by the models (without dust). The bar of model P seems the least realistic. It is a hybrid of power-law and Gaussian models along its major axis. The index of the power law is 5.0, higher than the values of ~ 3–4 often used in models of the Galactic halo but is not much higher than the best power-law fits of Stanek et al. (1997), in which $\rho \sim R^{-4}$. The bar/disk luminosity fraction is 0.56, and while estimates of this quantity vary greatly with galaxy and with measurement technique, the typical value for an early-type galaxy seems to be less than half this (Sellwood & Wilkinson 1993). The appearance of the bar is also unusual in that its outer isophotes lie parallel to the X'-axis for most of the bar's length but come to a point at its ends rather than forming a blunt, boxy terminus.

The outermost contours of the model E bar are not as pointed as those of model P but not as rectangular as one might expect. The bar/disk luminosity ratio is a plausible 0.33. The power of the exponential, 1.44, is intermediate between those of the best models of Dwek et al. (1995) and Stanek et al. (1997). This is my second-best model, on the bases of figure of merit and of my subjective evaluation of its appearance.

My preferred model is model S. Its bar is slightly shorter than the model E bar and tilted through a slightly greater angle. Its bar/disk luminosity ratio is 0.33, and its outer isophotes are clearly rectangular. The isophotes in its interior are diamond-shaped, with $C_\perp = 1.57$. This contrasts with the findings of Athanassoula et al. (1990) that $C_\perp =$ 2–4 in the bars of SB0 galaxies. They warn that an apparent $C_\perp < 2.0$ might result from the unintentional inclusion of a nuclear component that projects onto a circular area or onto an elliptical area with the long axis normal to the bar. To test for this, I excluded pixels within first 5°, then 6°, and then 7° of the Galactic center, refitting model S each time. When the exclusion radius increased, there was no significant change in $C_\perp$, so contamination by a nuclear component is probably not important. From the residual plots already shown, such a component may well exist, but it would have a much smaller scale height than the bar.

Diamond-shaped isophotes are not uncommon in bars, however. In the simulations of Contopoulos et al. (1989), orbits near the center of a bar are elliptical (the x_1 family of orbits), farther out they are increasingly diamond-shaped, and near the ends, they are rectangular (the 4:1 family of orbits). Quillen, Frogel, & Gonzalez (1994) also note a transition from diamond-shaped to rectangular orbits in NGC 4314 and suggest that it occurs at the $m = 4$ inner Lindblad resonance. Whether or not this is the case, the contour plot of model S in Figure 14 resembles that of NGC 4314 in Quillen et al. (1994). Athanassoula (1996) wondered if bars would appear as boxy in the near-infrared as in the B band. In the case of our Galaxy, the answer would seem to be, "Not quite."

With a $C_\parallel$ of 3.5, the bar is definitely boxy when seen edge-on. In the best bar model of Dwek et al. (1995), $C_\parallel \equiv$ 4.0. In this model (which they label "G2"), $C_\perp \equiv 2.0$, the bar power $n \equiv 2.0$, and the bar cutoff is fixed at either 2.4 kpc (from Binney et al. 1991) or 5.0 kpc (from Weinberg 1992); however, with a scale length $a_x \sim 1.7$ kpc, any cutoff beyond 3.5 kpc is probably moot. Instead of modeling the disk, they

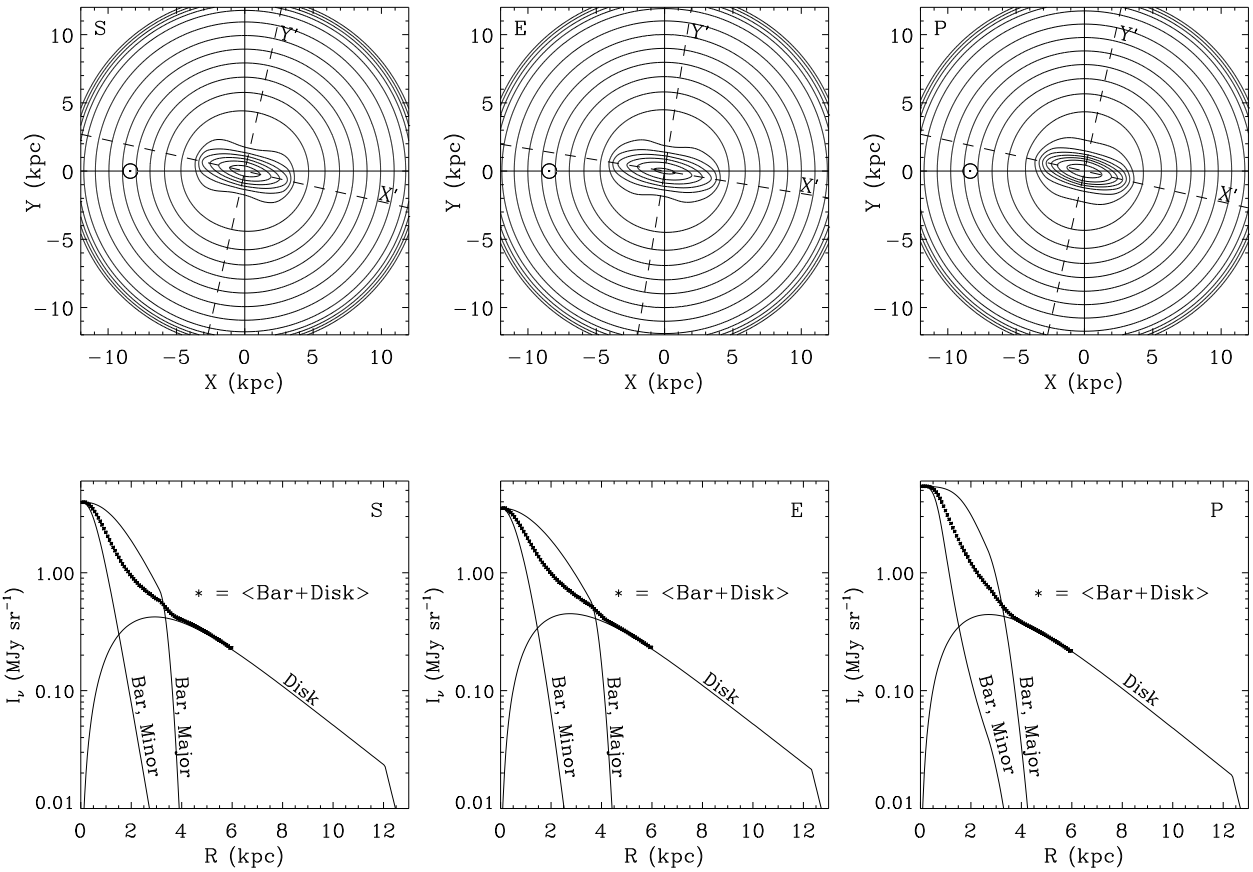

FIG. 14.—*Top*: Log of the face-on surface brightness from models S, E, and P. Our position is marked by the solar symbol. *Bottom*: *L*-band profiles taken along the major and minor axes of the bar. The asterisks denote an average of the bar plus the disk over the azimuth.

extrapolated its surface brightness in the DIRBE maps inward from larger longitudes to the region of the bulge (since the extrapolation did not take into account a central hole in the disk, this probably produced an overestimate). To further minimize the effects of the disk, they chose a relatively small bulge region with $3° < |b| < 10°$ and $|l| < 10°$. The *K*, *L*, and *M* bands were fitted individually, with the χ^2 as the figure of merit. The agreement between our results is fairly good, despite the differences in method. Taking their best (and most consistent) model, G2 with a 5 kpc cutoff, and ignoring the *K* band, which differs greatly in scale lengths from the other two, we find a tilt angle of 9°.5 and axis ratios of 1.75:0.62:0.42 kpc. The tilt angle and the ratio of scale lengths agree with those of my models. However, other Dwek et al. models that have values of χ^2 nearly as good as G2 lead to very dissimilar bars. I believe fewer and more general models would have produced more consistent and realistic bars. Some (such as Kuijken 1996) have commented on the inherent limitations in using surface photometry to reconstruct a three-dimensional bar. The problem is admittedly challenging, but we should not underestimate the amount of information offered by the DIRBE maps; even a 47 parameter model may be far from exhausting it.

The Stanek et al. (1997) results are more consistent than those of Dwek et al. (1995), at least in tilt angle. They applied the Dwek et al. models and several of their own to the distribution of "red clump" giants, which have a narrow range of intrinsic luminosity, in 12 fields toward the bulge. They assumed $R_0 \equiv 8.0$ kpc. All the Stanek et al. models returned a tilt angle $\sim 20°$ (14°–34°). Their best models were power-law and exponential models. The power-law models {exemplified by their model "P2" using $\rho \propto [R(1 + R)]^{-2}$} had axis ratios of 1.10:0.45:0.29 kpc. The exponential models ["E2": $\rho \propto \exp(-R)$} had axis ratios of 0.94:0.34:0.26 kpc. Their Gaussian model, similar to the Dwek et al. G2 model, had axis ratios of 1.33:0.56:0.45 kpc. Their coverage of the area of the bulge is still sparse; only six distinct directions were sampled, only two outside the latitude strip $-5° < b < -3°$.

The bar postulated by Binney et al. (1991) is tilted only a degree or two more from the Sun-center line than my model S bar but is significantly smaller and weaker. The bar is of the power-law type, ending within a corotation radius fixed at 2.4 kpc. It is unclear how the existence of a bar like that of model S would affect their interpretation of gas orbits in the inner Galaxy.

Profiles of the disk and bar along the major and minor axes of the bar are shown in Figure 14, along with profiles obtained by averaging the disk and the bar over the azimuth angle. In models S and E, the averaged profile remains approximately exponential as it continues inward in *R*. Ohta et al. (1990) found this to be true in their sample of barred spiral galaxies and cited it as evidence that the bar formed from an instability of the disk, with little redistribution of stars in the radial direction. The similarity in the near-infrared color of the bar and the disk also supports this theory (if we normalize the central emissivities to their *L*-band values, we get 2.33, 1.89, 1.0, and 0.51, respectively, for the *J* through *M* bands in the disk and 2.26, 1.93, 1.0,

and 0.50, respectively, in the bar). The greater scale height of the bar, 0.43 kpc versus 0.34 kpc for the disk, is consistent with the theory of Noguchi (1996) that early-type bars form from an already mature and thickened Galactic disk.

The type I disk models are shown in Figure 15. When the disk is not permitted a hole, the bar becomes less luminous (20% of the disk luminosity) and very diamond-shaped ($C_\perp = 1.28$). Neither the face-on views nor the profiles seem credible.

5.6. *The Parameter R_0*

All models showed a slight sensitivity to R_0 in their figures of merit, but only in the disk region. This can probably be attributed to extraneous factors, namely zodiacal light residue or an artifact of its removal, or to large-angle features of the young disk. To see how the values of the model parameters depend on our distance from the Galactic center, I repeated model S for values of R_0 spanning the range 7.5–9.5 kpc, approximately the range found in the current literature (see Reid 1993 for a review). The results are listed in Table 4. The formal errors have been omitted, but they are similar to those given by Table 2 for $R_0 =$ 8.5 kpc.

Most of the parameters are dependent on R_0 in a simple way, and it might be possible to determine R_0 if one of these parameters were known with confidence through some other means, but at present they are at least as uncertain as R_0. One parameter that might provide a lower limit is the extinction at the Sun's position. At $R_0 = 7.5$ kpc, the local J-band extinction is only 0.066 mag kpc^{-1}, and if the power law of extinction were extended to the V band, it would lead to an extinction of 0.3 V mag kpc^{-1}, one-half of what is considered a reasonable value. How significant is this discrepancy? One could argue that the term "local" is open to interpretation when dealing with something as patchy as extinction or that, by masking directions with high optical depths, I may have introduced a bias toward underestimating A_J, but I think it very probable that $R_0 > 7.5$ kpc. No such discrepancy is obvious at the high end, $R_0 = 9.5$ kpc, though; for this distance, the bar becomes uncomfortably diamond-shaped, with a face-on shape parameter $C_\perp = 1.48$.

5.7. *Luminosities*

In Paper I, I fitted a Planck curve to the central emissivities of the disk, deriving an effective temperature of 3800 K and using this to estimate the total luminosity of the old stellar disk. Since the colors are virtually unchanged and are the same for the bar and the disk, the same is done here for the disk plus bar (according to model S). Weighted by a 3800 K blackbody spectrum, the effective frequencies of the DIRBE J, K, L, and M bands are, respectively, 2.38, 1.36, 0.864, and 0.615×10^{14} Hz. The effective widths of the bandpasses are 5.85, 2.22, 2.18, and 0.828×10^{13} Hz, respectively. For $R_0 = 8.5$ kpc, the respective luminosities are 39.2, 12.2, 6.3, and $1.2 \times 10^8\ L_\odot$. Calculating the bolometric corrections for the four bands and averaging them using the weights in Table 1, we obtain the luminosities of the disk

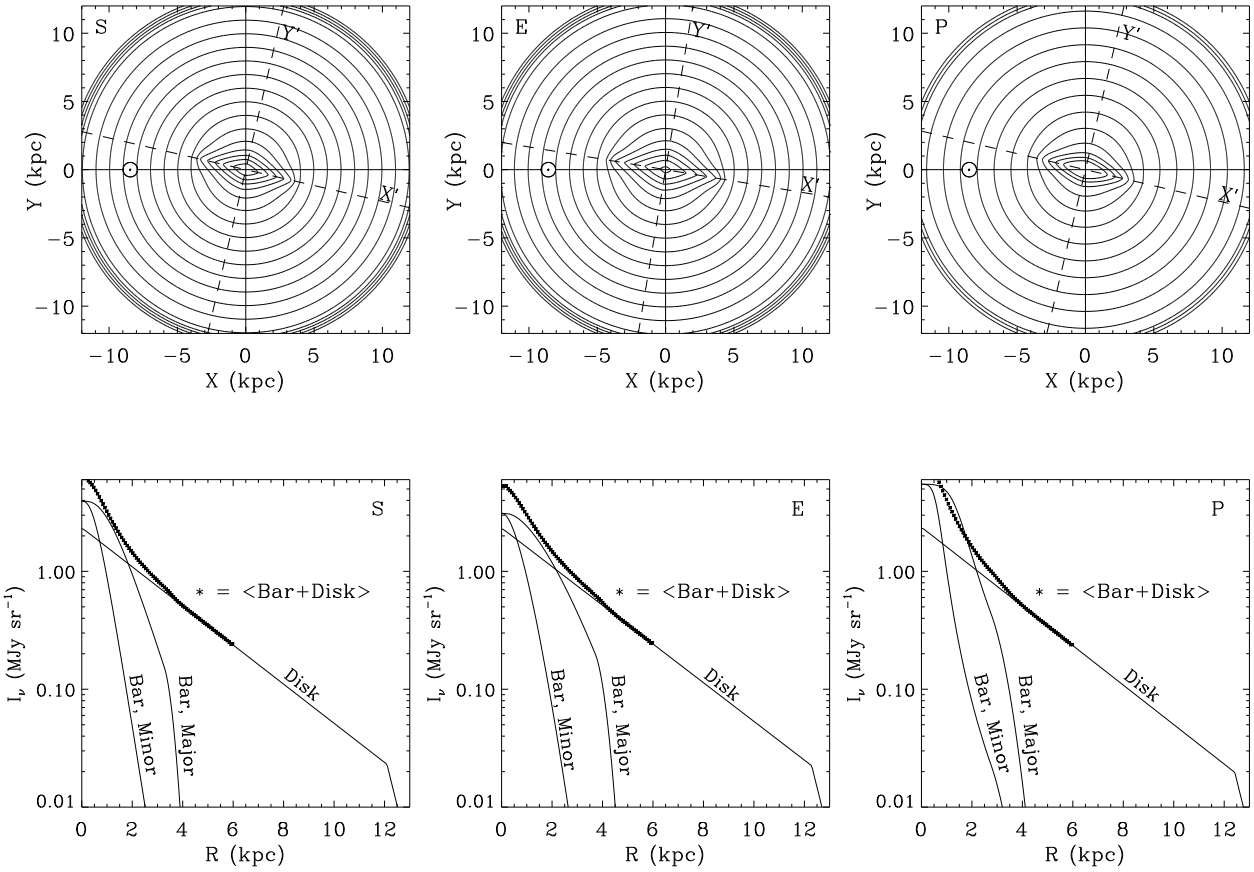

FIG. 15.—*Top*: Log of the face-on surface brightness from models S, E, and P with no hole in the disk. Our position is marked by the solar symbol. *Bottom*: L-band profiles taken along the major and minor axes of the bar. The asterisks denote an average of the bar plus the disk over the azimuth.

TABLE 4

MODEL S VERSUS R_0, USING THE PRIMARY MASK

PARAMETER	DISTANCE TO GALAXY CENTER R_0 (kpc)				
	7.5	8.0	8.5	9.0	9.5
Distance to Galaxy plane Z_0 (pc)	14.90	16.08	16.46	16.27	16.69
Bar tilt angle θ_0 (deg)	13.69	12.86	13.79	14.58	15.02
Disk scale length h_r (kpc)	2.3504	2.476	2.6045	2.7092	2.8305
Disk scale height h_z (kpc)	0.3196	0.3340	0.3457	0.3602	0.3719
Disk radius $R_{\max}$ (kpc)	11.61	12.11	12.18	12.87	13.35
Warp line of nodes ϕ_W (deg)	0.51	0.48	0.44	0.52	0.48
Disk $\rho_J(0)$ (MJy sr^{-1} kpc^{-1})	8.213	8.272	8.157	8.144	8.088
Disk $\rho_K(0)$ (MJy sr^{-1} kpc^{-1})	6.725	6.731	6.648	6.666	6.671
Disk $\rho_L(0)$ (MJy sr^{-1} kpc^{-1})	3.586	3.527	3.511	3.513	3.506
Disk $\rho_M(0)$ (MJy sr^{-1} kpc^{-1})	1.806	1.781	1.782	1.745	1.746
Disk-hole radius O_R (kpc)	2.733	2.939	2.973	2.971	2.998
Disk-hole power O_N	1.729	1.721	1.711	1.784	1.796
Hole axis ratio ε	0.855	0.870	0.8554	0.955	0.849
Bar pitch angle (deg)	−0.01	0.036	−0.023	−0.159	−0.170
Bar X scale length a_x (kpc)	1.581	1.693	1.696	1.763	1.817
Bar Y scale length a_y (kpc)	0.5736	0.6266	0.6426	0.6734	0.7102
Bar Z scale length a_z (kpc)	0.3970	0.4172	0.4425	0.471	0.4966
Bar cutoff radius $R_{\rm end}$ (kpc)	2.631	2.967	3.128	3.315	3.509
Bar cutoff scale length $h_{\rm end}$ (kpc)	0.451	0.440	0.461	0.445	0.509
Bar face-on shape $C_\perp$	1.634	1.550	1.574	1.516	1.478
Bar edge-on shape $C_\parallel$	3.446	3.427	3.501	3.352	3.279
Bar $\rho_J(0)$ (MJy sr^{-1} kpc^{-1})	10.75	10.65	10.52	10.48	10.38
Bar $\rho_K(0)$ (MJy sr^{-1} kpc^{-1})	8.942	8.849	8.817	8.79	8.738
Bar $\rho_L(0)$ (MJy sr^{-1} kpc^{-1})	4.676	4.581	4.538	4.484	4.470
Bar $\rho_M(0)$ (MJy sr^{-1} kpc^{-1})	2.360	2.286	2.255	2.234	2.199
Dust scale length h_r^d (kpc)	2.688	2.981	3.066	3.249	3.387
Dust Scale Height h_z^d (kpc)	0.1575	0.1500	0.1520	0.180	0.194
Dust warp factor x^d	1.787	1.796	1.782	1.778	1.757
Local extinction A_J (J mag kpc^{-1})	0.0656	0.1050	0.1144	0.1209	0.1311
Extinction index α	1.887	1.783	1.787	1.740	1.696
Dust hole radius O_R^d (kpc)	2.624	2.585	2.615	2.623	2.636
Dust hole power O_N^d	2.131	2.102	2.150	2.093	2.102
Dust $\rho_J(0)$ (MJy sr^{-1} kpc^{-1})	4.702	4.652	4.642	4.614	4.625
Dust $\rho_K(0)$ (MJy sr^{-1} kpc^{-1})	1.147	1.161	1.152	1.135	1.131
Dust $\rho_L(0)$ (MJy sr^{-1} kpc^{-1})	2.244	2.187	2.180	2.157	2.148
Dust $\rho_M(0)$ (MJy sr^{-1} kpc^{-1})	2.360	3.213	3.236	3.179	3.148
Total Luminosity ($\times 10^{10}$ $L_\odot$)	1.9	2.1	2.3	2.7	3.0

NOTE.—The emissivities ρ are given in uncommon units but can be converted using 1 MJy sr^{-1} kpc^{-1} = 9.522×10^9 W pc^{-3} Hz^{-1} sr^{-1}.

and bar. Their sum is given is the last row of Table 4; for $R_0 = 8.5$ kpc, the total luminosity is 2.3×10^{10} $L_\odot$. There is little change when switching to model E or the minimal mask; the total luminosity varies by less than 4% among the two bar models and two masks.

6. CONCLUSIONS

The old stellar disk is approximated well by a function that is exponential in R and sech^2 in Z. It is warped similarly to the H I layer and has an outer edge and a central hole. The stellar emissivity peaks at approximately the inner radius of the 3 kpc ring of molecular clouds and is truncated approximately 4 kpc beyond the solar circle. The dust layer also has a central hole, slightly smaller but sharper than that of the disk. If $R_0 = 8.5$ kpc, the scale length of the disk is 2.60 kpc, the scale height is 0.34 kpc, and the Sun is located 16.5 pc above its midplane.

I have modeled the Galaxy's bar using three types of function, a power-law-with-a-core function, an exponential-to-a-power function, and a sech^2 function. Of these, the sech^2 function provided the best fit, but all three bar models agree on several points: the bar is strong and truncated at approximately the radius of the hole; it has the same color as the disk, but a larger scale height; and the bar lies in the plane of the Galaxy and is tilted 9°–15° from the line between the Sun and the Galactic center. There is probably a nuclear component with a scale length of ~100 pc in addition to the disk, the bar, and those features attributable to the young disk, such as giant molecular clouds, spiral arms, and possibly a bar-circling ring.

Model S, the "sech^2" bar, is the best model in terms of figure of merit, simplicity, and similarity to other barred spiral galaxies. According to this model, if $R_0 = 8.5$ kpc, the bar has axis ratios of 1.70:0.64:0.44 kpc. It is tilted 14° and is one-third as luminous (in the near-infrared) as the disk. Other characteristics of the bar, the disk, and the dust layer are presented in Table 4.

How much faith can be placed in these results? The most distinguishing feature of my model is probably its versatility. It allows the Galactic disk to warp and to have an inner hole and a sharp outer edge. It allows the bar to have its own truncation and a different "boxiness" when viewed from above or from the plane of the disk. Nevertheless, the model is not infinitely flexible, nor is it provably the best. Yet I find the similarity in the end products of the three bar models encouraging. Despite the constraints of their different functional forms, they seem to be converging on a single destination. There is no reason to believe that even the best

of them has arrived at that destination, but the bar models' self-consistency, plausible parameter values, and small, mostly explainable, residuals argue that they have come close.

COBE is supported by NASA's Astrophysics Division. Goddard Space Flight Center, under the scientific guidance of the *COBE* Science Working Group, was responsible for the development and operation of *COBE*. The author is grateful to the *COBE* team and wishes to express special thanks to the surviving DIRBE researchers, Rick Arendt, Nils Odegard, and Janet Weiland. I also extend my thanks to the anonymous referee.

REFERENCES

Athanassoula, E. 1992a, MNRAS, 259, 328
———. 1992b, MNRAS, 259, 345
———. 1996, in Spiral Galaxies in the Near-IR, ed. D. Minniti & H.-W. Rix (Berlin: Springer), 147
Athanassoula, E., Morin, S., Wozniak, H., Puy, D., Pierce, M. J., Lombard, J., & Bosma, A. 1990, MNRAS, 245, 130
Baggett, W. E., Baggett, S. M., & Anderson, K. S. J. 1996, in IAU Colloq. 157, Barred Galaxies, ed. R. Buta, D. A. Crocker, & B. G. Elmegreen (San Francisco: ASP), 91
Bahcall, J. N., & Soneira, R. M. 1980, ApJS, 44, 73
Binney, J., Gerhard, O. E., Stark, A. A., Bally, J., & Uchida, K. I. 1991, MNRAS, 252, 210
Blitz, L., & Spergel, D. N. 1991, ApJ, 379, 631
Boggess, N. W., et al. 1992, ApJ, 397, 420
Burbridge, G. R., & Hoyle, F. 1963, ApJ, 138, 57
Burton, W. B. 1976, ARA&A, 14, 275
Buta, R. 1986, ApJS, 61, 609
Calbet, X., Mahoney, T., Hammersley, P. L., Garzón, F., & Lopez-Corredoira, M. 1996, ApJ, 457, L27
Contopoulos, G., Gottesman, S. T., Hunter, J. H., & England, M. N. 1989, ApJ, 343, 608
Dame, T. M., et al. 1987, ApJ, 322, 706
de Vaucouleurs, G. 1964, in IAU Symp. 20, The Galaxy and the Magellanic Clouds, ed. F. J. Kerr & A. W. Rogers (Canberra: Australian Acad. Sci.), 195
de Vaucouleurs, G., & Pence, W. D. 1978, AJ, 83, 1163
Dickey, J. M., & Lockman, F. J. 1990, ARA&A, 28, 215
Dwek, E., et al. 1995, ApJ, 445, 716
Elmegreen, B. G., & Elmegreen, D. M. 1985, ApJ, 288, 434
Elmegreen, B. G., Elmegreen, D. M., Chromey, F. R., Hasselbacher, D. A., & Bissell, B. A. 1996, AJ, 111, 2233
Freeman, K. C. 1970, ApJ, 160, 811
Freudenreich, H. T. 1996, ApJ, 468, 663 (Paper I)
Freudenreich, H. T., et al. 1994, ApJ, 429, L69
Gerhard, O. E., & Vietri, M. 1986, MNRAS, 223, 377
Hammersley, P. L., Garzón, F., Mahoney, T., & Calbet, X. 1994, MNRAS, 269, 753
Harmon, R., & Gilmore, G. 1988, MNRAS, 235, 1025
Hohl, F. 1971, ApJ, 168, 343
Kent, S. M. 1992, ApJ, 387, 181
Kormendy, J. 1977, ApJ, 227, 714
Kuijken, K. 1996, in IAU Colloq. 157, Barred Galaxies, ed. R. Buta, D. A. Crocker, and B. G. Elmegreen (San Francisco: ASP), 504
Liszt, H. S., & Burton, W. B. 1980, ApJ, 236, 779
Matsumoto, T., et al. 1982, in AIP Conf. Proc. 83, The Galactic Center, ed. G. R. Riegler & R. D. Blandford (New York: AIP), 48
Morris, M., & Serabyn, E. 1996, ARA&A, 34, 645
Nakada, Y., Deguchi, S., Hashimoto, O., Izumiura, H., Onaka, T., Sekiguchi, K., & Yamamura, I. 1991, Nature, 353, 140
Noguchi, M. 1996, ApJ, 469, 605
Ohta, K., Hamabe, M., & Wakamatsu, K. 1990, ApJ, 357, 71
Oort, K., Kerr, F. J., & Westerhout, G. 1958, MNRAS, 118, 379
Paczyński, B., Stanek, K. Z., Udalski, A., Szymański, M., Kałużny, J., Kubiak, M., Mateo, M., & Krzemiński, W. 1994, ApJ, 435, L113
Press, W. H., Teukolsky, S. A., Vettering, W. T., & Flannery, B. P. 1992, Numerical Recipes in Fortran (2d ed.; New York: Cambridge Univ. Press)
Quillen, A. C., Frogel, J. A., & Gonzalez, R. A. 1994, ApJ, 437, 162
Reid, M. J. 1993, ARA&A, 31, 345
Rieke, G. H., & Lebofsky, M. J. 1985, AJ, 288, 618
Robin, A. C., Crézé, M., & Mohan, V. 1996, in IAU Symp. 169, Unsolved Problems of the Milky Way, ed. L. Blitz & P. Teuben (Dordrecht: Kluwer), 681
Sanders, R. H., & Prendergast, K. H. 1974, ApJ, 188, 489
Schwartz, M. P. 1984, MNRAS, 209, 93
Sellwood, J. A., & Wilkinson, A. 1993, Rep. Prog. Phys., 56, 173
Stanek, K. Z., Udalski, A., Szymański, M., Kałużny, J., Kubiak, M., Mateo, M., & Krzemiński, W. 1997, ApJ, 477, 163
Valée, J. P. 1995, ApJ, 454, 119
Weiland, J. L., et al. 1994, ApJ, 425, L81
Weinberg, M. D. 1992, ApJ, 384, 81
Whitelock, P., & Catchpole, R. 1992, in The Center, Bulge, and Disk of the Galaxy, ed. L. Blitz (Dordrecht: Kluwer), 103
Zhao, H. 1996, MNRAS, 278, 488

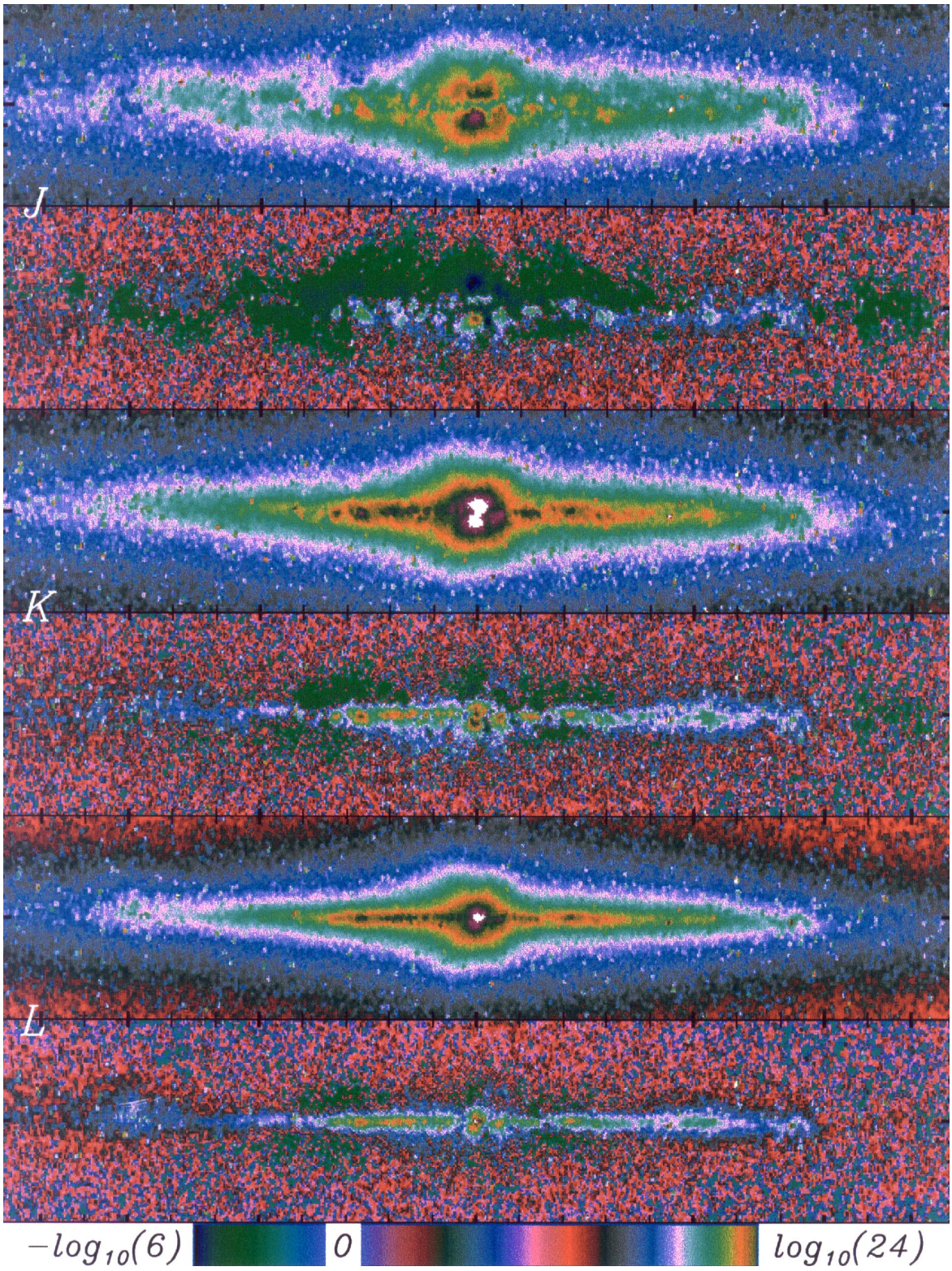

FIG. 9.—*J*-, *K*-, and *L*-band surface brightnesses [log ($|I_\nu| + 0.001$ MJy sr^{-1})] before and after the model S map was subtracted. The colors of this coded intensity image are modulated to create a contour-like effect to better show structure. Colors to the left of the break in the color bar (blue to dark green to blue) represent negative surface brightness. White pixels are saturated. The range is $l < 110°$ and $b < 15°$. Tick marks are at intervals of 10° (*l*) and 3° (*b*).

FREUDENREICH (see 492, 503)

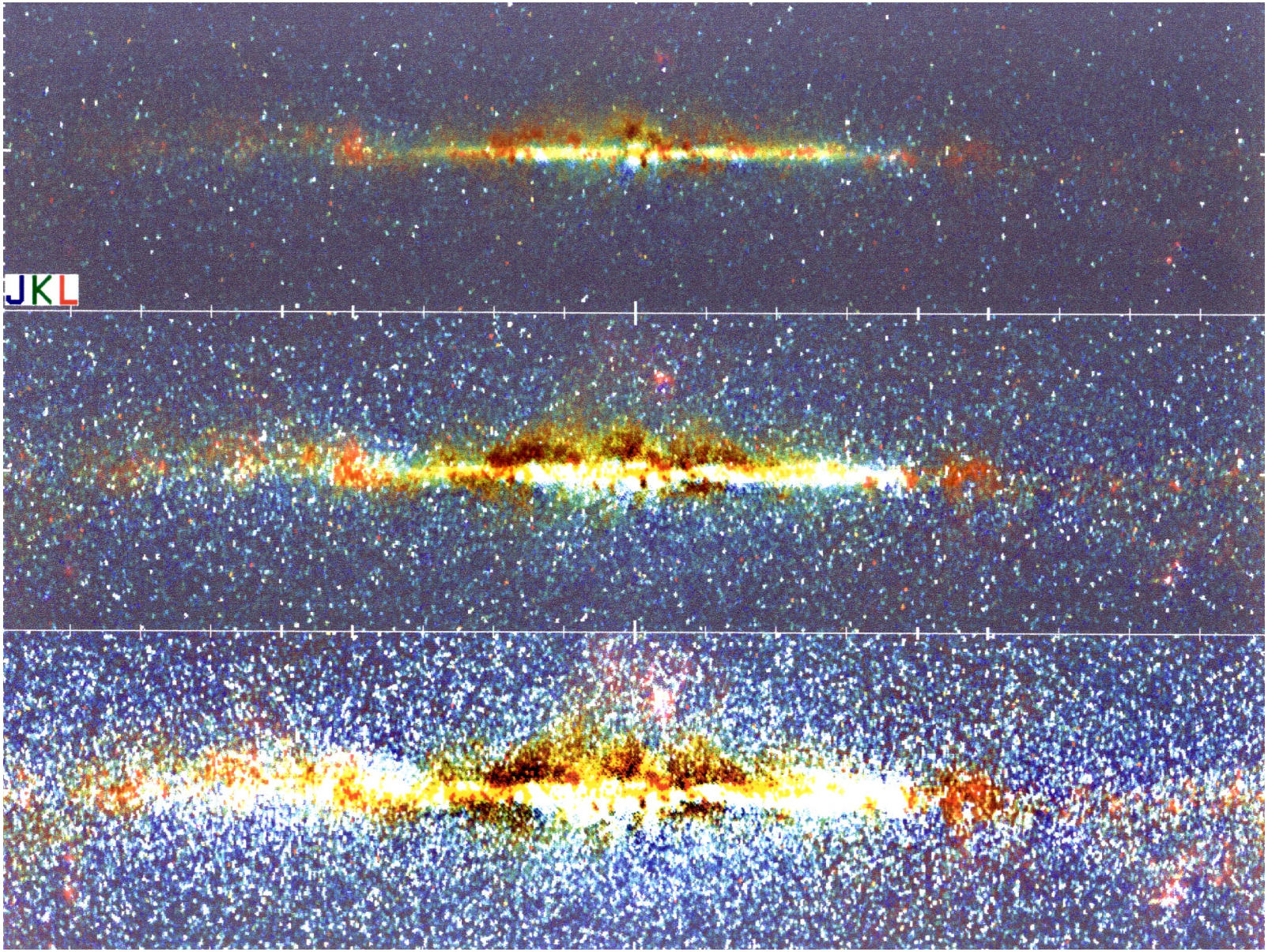

FIG. 10.—Three-color image of the Galaxy ($|b| < 45°$) after model S was subtracted. The modeled J and K bands have been scaled to have the same central emissivity as the L band so that all three have equal weight. *Top*: $I_\nu = -2.5$–2.5 MJy sr^{-1}. *Middle*: $I_\nu = -0.5$–0.5 MJy sr^{-1}. *Bottom*: $I_\nu = -0.1$–0.1 MJy sr^{-1}. Tick marks are at intervals of 10° (l) and 5° (b). The faint pebbled texture of the bottom panel is caused by point-source residuals.

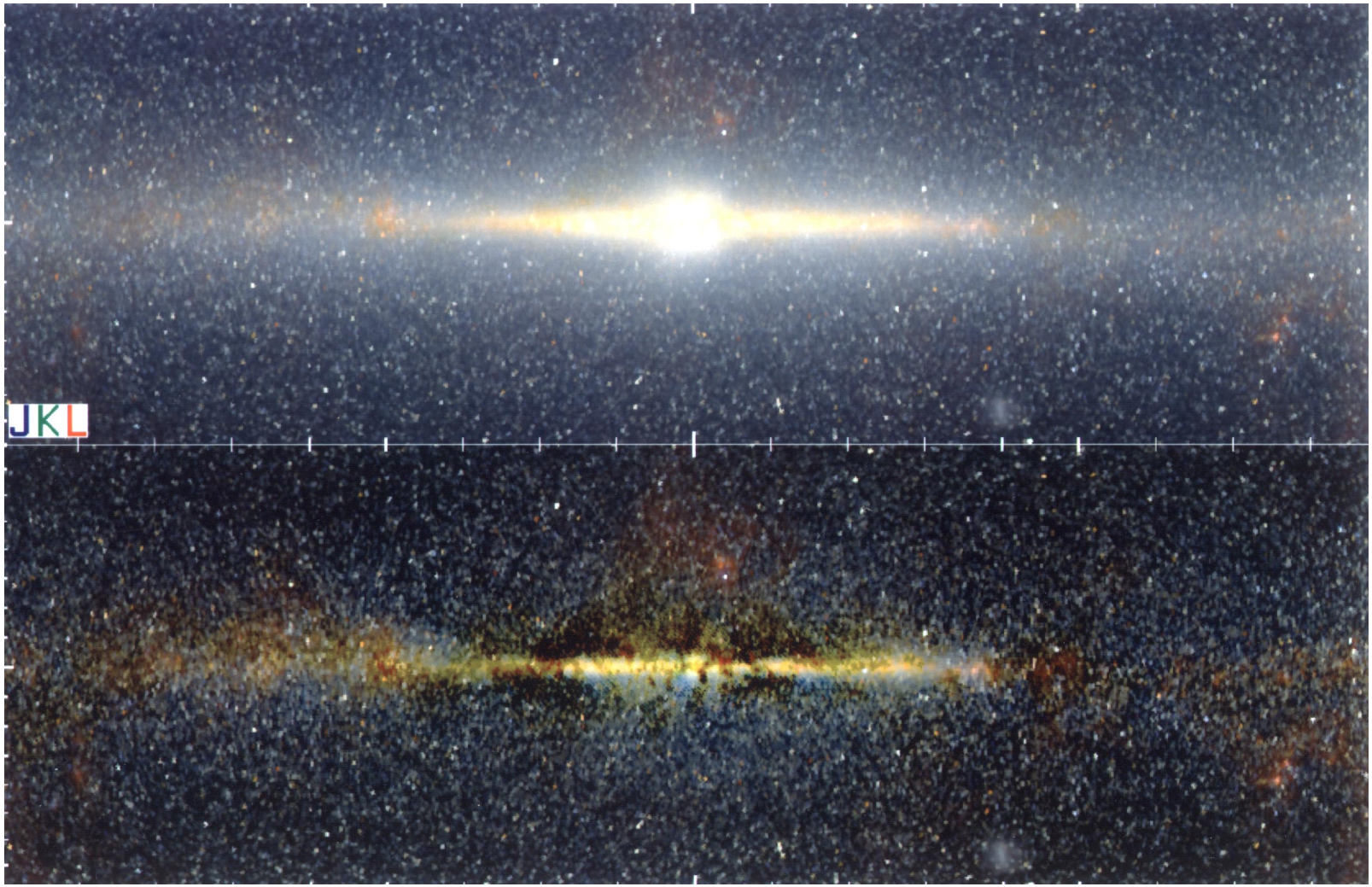

FIG. 11.—Logarithmic three-color image of the Galaxy ($|b| < 60°$) before and after model S was subtracted. The J and K bands have been scaled to the central emissivity of the L band. Tick marks are at intervals of 20° (l) and 5° (b).